NASA Tech Briefs

National Aeronautics and
Space Administration

Electronic Components and Circuits

Electronic Systems

Physical Sciences

Materials

Computer Programs

Mechanics

Machinery

Fabrication Technology

Mathematics and Information Sciences

Life Sciences

July 1998

INTRODUCTION

Tech Briefs are short announcements of new technology derived from the research and development activities of the National Aeronautics and Space Administration. These Briefs emphasize information considered likely to be transferable across industrial, regional, or disciplinary lines and are issued to encourage commercial application.

Availability of NASA Tech Briefs and TSP's

Distribution of NASA Tech Briefs, a monthly periodical publication, is limited to engineers in U.S. Industry and to other domestic technology transfer agents. Requests for individual Tech Briefs or for Technical Support Packages (TSP's) announced herein should be addressed to

NASA Center for AeroSpace Information
Technology Transfer Office
800 Elkridge Landing Rd.
Linthicum Heights, MD 21090-2934
Telephone No. (301) 621-0245

Please reference the three-letter, five-digit control number located at the end of each Tech Brief. Information on NASA's Technology Utilization Program, its documents, and services is also available at the same facility.

Technology Utilization Officers and Patent Counsels are located at NASA field installations to provide technology-transfer access to industrial users. Inquiries can be made by writing to NASA field installations listed below.

Technology Utilization Officers and Patent Counsels

Ames Research Center
Technology Utilization Officer
Mail Code 223-3
Moffett Field, CA 94035

Patent Counsel
Mail Code 200-11
Moffett Field, CA 94035

Goddard Space Flight Center
Technology Utilization Officer
Mail Code 702-1
Greenbelt, MD 20771

Patent Counsel
Mail Code 204
Greenbelt, MD 20771

Lyndon B. Johnson Space Center
Technology Utilization Officer
Mail Code IC-4
Houston, TX 77058

Patent Counsel
Mail Code AL3
Houston, TX 77058

John F. Kennedy Space Center
Technology Utilization Officer
Mail Stop PT-PMO-A
Kennedy Space Center, FL 32899

Patent Counsel
Mail Code PT-PAT
Kennedy Space Center, FL 32899

Langley Research Center
Technology Utilization Officer
Mail Stop 143
Hampton, VA 23665

Patent Counsel
Mail Code 279
Hampton, VA 23665

Lewis Research Center
Technology Utilization Officer
Mail Stop 7-3
21000 Brookpark Road
Cleveland, OH 44135

Patent Counsel
Mail Code LE-LAW
21000 Brookpark Road
Cleveland, OH 44135

Jet Propulsion Laboratory
Technology Utilization Officer
Mail Stop 156-211
4800 Oak Grove Drive
Pasadena, CA 91109

NASA Resident Office-JPL
Technology Utilization Officer
Mail Stop 180-801
4800 Oak Grove Drive
Pasadena, CA 91109

Patent Counsel
Mail Code 180-801
4800 Oak Grove Drive
Pasadena, CA 91109

George C. Marshall Space Flight Center
Technology Utilization Officer
Code AT01
Marshall Space Flight Center, AL 35812

Patent Counsel
Mail Code CC01
Marshall Space Flight Center, AL 35812

John C. Stennis Space Center
Technology Utilization Officer
Code HA-30
Stennis Space Center, MS 39529

NASA Headquarters
Technology Utilization Officer
Code CU
Washington, DC 20546

Assistant General Counsel for Patent Matters
Code GP
Washington, DC 20546

Dryden Flight Research Center
Technology Utilization Officer
M/S D21-31
Bldg. 4832 Whse 7
Lilly Dr.
Edwards, CA 93523

NASA TechBriefs

National Aeronautics and Space Administration

July 1998
98-07

BLANK PAGE

Electronic Components and Circuits

Hardware, Techniques, and Processes

BLANK PAGE

Inverse Rectennas for Two-Way Wireless Power Transmission

Suitable rectennas under reverse bias can be made to act as transmitters.

NASA's Jet Propulsion Laboratory, Pasadena, California

The term "inverse rectenna" may seem like an oxymoron at first glance. However, preliminary experiments have demonstrated that a rectenna of suitable design can be made to operate in an inverse mode, in which radio-frequency (RF) power is generated in the rectenna rectifier circuits and radiated by the rectenna antenna elements.

This experimental finding provides encouragement for the use of rectennas as bidirectional (both transmitting and receiving) devices in developmental microwave wireless-power-transmission systems. Heretofore, a bidirectional microwave terminal for a typical conceptual wireless-power-transmission system might have included (a) a transmitter comprising a transmitting antenna connected to a magnetron or klystron oscillator or perhaps an impact avalanche transit-time- (IMPATT)-diode oscillator, plus (b) a receiver comprising a separate rectenna. If only one device — a rectenna capable of operating in transmitting as well as receiving mode — could be used at each end of a microwave power link, then the cost of the link could be reduced. Potential applications for inverse rectennas lie in the microwave wireless transmission of power between any two of the following: ground stations, airships, aircraft, and spacecraft.

In the rectenna used in the experiments, the rectifier circuits included low-pass microwave filters and microwave resonators connected to GaAs Schottky-barrier diodes (see figure). Inverse operation was obtained by doing little more than treating the dc-output terminals as dc-input terminals. By simply applying reverse-polarity dc bias to these terminals, the rectifier circuits were made to function similarly to IMPATT-diode oscillators.

Approximately, 1 percent dc to RF conversion efficiency was obtained, with oscillations at 3.3 GHz. In previous research, rectenna energy-conversion efficiency as high as 91 percent had been achieved in the receiving mode. However, IMPATT oscillators are typically only about 10-percent efficient; in other words, about 90 percent of the dc input power becomes heat, which must be removed. Special provisions for heat sinking were made for the experiments. The issues of energy-conversion efficiency and heat sinking would have to be addressed in developing practical inverse rectennas.

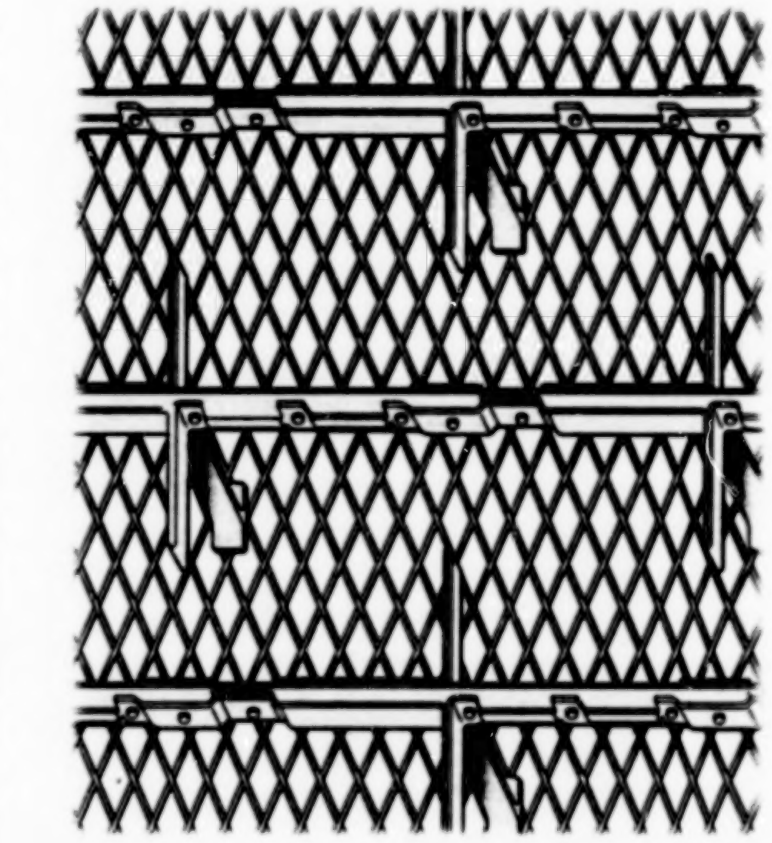

SIMPLIFIED ELECTRICAL SCHEMATIC DIAGRAM OF ONE UNIT

This Rectenna Array consists of multiple identical units, each containing dipole microwave antenna elements, microwave circuitry, and a half-wave rectifier in the form of a GaAs Schottky-barrier diode. In the traditional mode of operation, the array acts as a receiver, converting incident RF power to dc power. In the recently discovered inverse mode, the array acts as a transmitter, converting dc power to radiated RF power.

This work was done by Richard M. Dickinson of Caltech and James McSpadden of Texas A&M, NASA Center for Space Power, for **NASA's Jet Propulsion Laboratory**. *Further information is contained in a TSP [see page 1].*

NPO-20321

Improved Two-Wavelength Focal-Plane Array of QWIPs

Temperatures of objects imaged on the array could be determined.

NASA's Jet Propulsion Laboratory, Pasadena, California

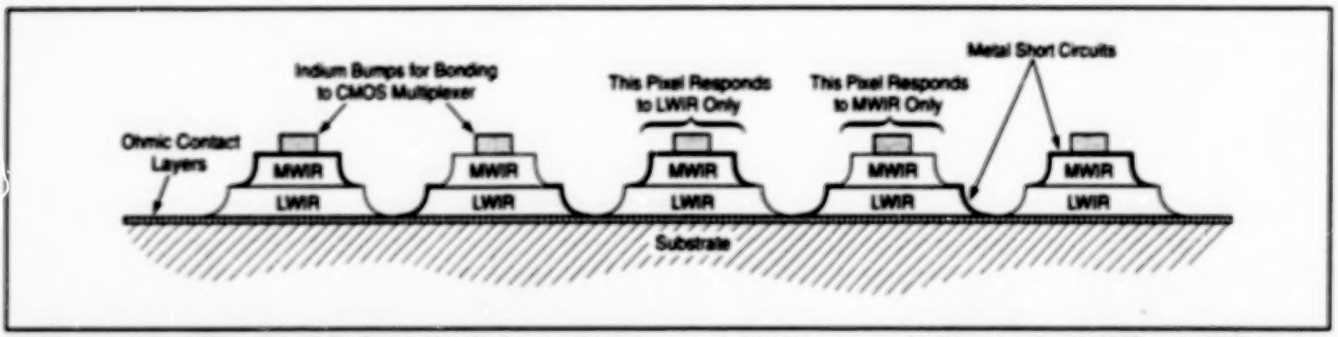

MWIR and LWIR QWIPs Would Be Short-Circuited in an alternate rows so that the array would detect interlaced LWIR and MWIR images. This is a schematic partial cross-sectional view looking along the rows.

A focal-plane array (FPA) of GaAs-based quantum-well infrared photodetectors (QWIPs) that would detect images in two wavelength bands simultaneously is undergoing development. From ratios between image intensities at the two wavelengths, one can calculate the temperatures of imaged objects by use of Planck's radiation law. In several respects, this device is similar to the one described in "Two-Wavelength Focal-Plane Array of QWIPs" (NPO-19658) *NASA Tech Briefs*, Vol. 22, No. 1 (January 1998), page 8a. Both devices are intended to serve as prototypes of multispectral imaging devices for a variety of scientific, industrial, and military infrared instruments.

QWIPs that operate in medium-wave infrared (MWIR) and long-wavelength infrared (LWIR) bands have been undergoing development in recent years. The best previously available two-wavelength QWIP contains two stacked, voltage-tunable QWIP structures — one for MWIR and one for LWIR. Two difficulties arise in connection with attempts to utilize that device in an FPA: (1) the device must be supplied with two voltages, which cannot be obtained from any currently available readout multiplexers; and (2) a high bias (>8V) must be supplied to the LWIR segment to switch on LWIR detection.

The present device is designed to overcome these difficulties. It is based partly on the QWIP FPA in a portable camera developed recently by the same innovators. The array would contain 512 × 484 pixels. Each pixel would contain 25 periods of an MWIR QWIP structure stacked with 25 periods of an LWIR QWIP structure. The two stacks would be separated by a heavily doped intermediate GaAs contact layer. The responses of the MWIR and LWIR QWIP structures would peak at wavelengths of 4.5 and 9 μm, respectively. This entire stack as described thus far would be sandwiched between doped GaAs contact layers and grown on a semi-insulated GaAs substrate by molecular-beam epitaxy. A GaAs cap layer would be added on top of a thin AlGaAs stop-etch layer on top of the device to fabricate a light-coupling optical cavity.

All pixels would contain both the MWIR and LWIR structures. However, during a metallization sequence that would be part of the fabrication process, the MWIR QWIPs on odd-numbered rows and the LWIR QWIPs on even-numbered rows of the FPA would be short-circuited (see figure). This interlaced short-circuiting of the MWIR and LWIR detectors would eliminate complicated voltage tuning and the necessity for very high bias voltage to operate the LWIR QWIPS. The QWIP FPA would be hybridized to a 512 × 484 complementary metal oxide/semiconductor (CMOS) multiplexer, which would read the alternating LWIR and MWIR rows to produce both an MWIR and an LWIR image of the same scene.

This work was done by Sarath D. Gunapala of Caltech and Kwong Kit Choi of the U.S. Army Research Laboratory for **NASA's Jet Propulsion Laboratory**. *Further information is contained in a TSP [see page 1].*

In accordance with Public Law 96-517, the contractor has elected to retain title to this invention. Inquiries concerning rights for its commercial use should be addressed to

Technology Reporting Office
JPL
Mail Stop 122-116
4800 Oak Grove Drive
Pasadena, CA 91109
(818) 354-2240

Refer to NPO-19837, volume and number of this NASA Tech Briefs *issue, and the page number.*

Delta-Doped CCDs as Low-Energy-Particle Detectors

Detection of particles is in addition to traditional use of CCDs as imaging devices.

NASA's Jet Propulsion Laboratory, Pasadena, California

Charge-coupled devices (CCDs) of a type developed previously for imaging in ultraviolet light have been found to be useful as detectors of electrons and other charged particles with kinetic energies as low as about 100 eV. Heretofore, solid-state electronic devices have generally not been useful for detecting particles with kinetic energies below the keV range. The devices in question are back-side-illuminated silicon CCDs with p⁺ delta (δ) doping at their back-side interfaces between silicon and surface layers of silicon dioxide. Such a device at an earlier stage of development was described in "Growth of δ-Doped Layer on Silicon

CCD" (NPO-18668) in the *Laser Tech Briefs* edition of *NASA Tech Briefs*, Vol. 19, No. 2 (February 1995), page 11.

When an energetic charged particle enters a detector, some of its kinetic energy is dissipated in the generation of electron/hole pairs; the problem is to collect and measure the electron/hole charges before the electrons and holes recombine. In the absence of δ doping, the inability of a silicon back-surface-illuminated device to detect either ultraviolet photons or low-energy charged particles is attributable to a "dead" layer that includes the surface SiO_2 plus a potential well that extends about 0.5 μm into the silicon from the Si/SiO_2 interface (see figure). The depth of penetration of the particles in the energy range of interest is less than the depth of the dead layer. Consequently, most of the electrons generated by impingement of charged particles become trapped in the potential well, where they eventually recombine with holes and thus go undetected.

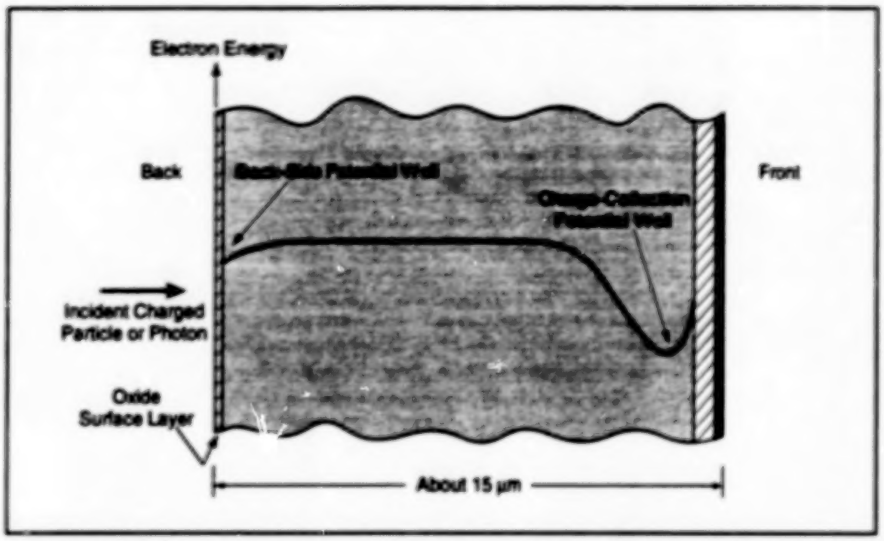

A Potential Well forms by trapping of positive charges in the oxide layer on the back side of a thin silicon CCD. The potential well captures electrons generated by impingement of low-energy charged particles from the back. Delta doping eliminates the back-surface potential well, making it possible to collect and measure the generated electrons.

Delta doping reduces the low-energy detection limit by effectively eliminating the back-side potential well. Delta doping is so named because its density-vs.-depth characteristic is reminiscent of the Dirac δ function (impulse function); the dopant is highly concentrated in a very thin layer. Preferably, the dopant is concentrated in one or at most two atomic layers in a crystal plane and therefore δ doping is also known as atomic plane doping.

An experimental δ-doped CCD for detecting low-energy charged particles was made by subjecting a commercial CCD to the following additional fabrication steps: First, an atomically clean silicon back surface was prepared by use of a hydrogen-termination surface-cleaning procedure that involves temperatures no more than about 200 °C. Then residues of the cleaning procedure were outgassed in a vacuum as the temperature of the device was gradually increased to an epitaxial-deposition temperature of 450 °C. A 1-nm-thick layer of silicon doped with boron [an acceptor (p) dopant] to a density of 4×10^{20} atoms/cm^3 was deposited epitaxially on the cleaned back surface. The silicon flux was interrupted briefly to enable the deposition of a δ layer of boron with an areal density of 2×10^{14} atoms/cm^2. The silicon flux was resumed to deposit a 1.5-nm-thick cap layer of silicon. Finally, the cap layer was exposed to steam to form a protective oxide on the back surface.

In experiments, the device was found to detect incident electrons with energies as low as 50 eV. Quantitative analysis was performed for incident electrons in the 200-to-1,000-eV range. The signal monotonically increased with increasing energy of the incident electrons. On the basis of data acquired in the experiments, it has been estimated that eventually, cooled, δ-doped CCDs should be able to detect single electrons with energies as low as 100 eV, at a noise limit of 3 electrons per pixel.

This work was done by Shouleh Nikzad, Michael Hoenk, and Michael Hecht of Caltech; Amy Smith of MIT; and Qiuming Yu of Kansas State University for **NASA's Jet Propulsion Laboratory**. *Further information is contained in a TSP [see page 1].*

In accordance with Public Law 96-517, the contractor has elected to retain title to this invention. Inquiries concerning rights for its commercial use should be addressed to

Technology Reporting Office
JPL
Mail Stop 122-116
4800 Oak Grove Drive
Pasadena, CA 91109
(818) 354-2240

Refer to NPO-20178, volume and number of this NASA Tech Briefs *issue, and the page number.*

Delta-Doped CCDs for Measuring Energies of Positive Ions

Kinetic energies as low as 1.25 keV can be measured.

NASA's Jet Propulsion Laboratory, Pasadena, California

Research closely related to that reported in the preceding article has shown that δ-doped charge-coupled devices (CCDs) could be used to detect incident protons and perhaps other positive ions, and to measure the kinetic energies of the ions, down to about 1.25 keV. Prior to the development of δ-doped CCDs, the minimum kinetic energy for detectability of protons by solid-state devices was about 10 keV, for the reasons described in the preceding article.

Heretofore, a typical instrument for detecting low-kinetic-energy charged particles and measuring the particle kinetic energies has comprised a relatively heavy, power-hungry electrostatic- or magnetic-energy analyzer followed by a microchannel-plate detector. In contrast, δ-doped CCDs offer the capability for measuring kinetic energies directly in the detection process, without need for electrostatic or magnetic energy analyzers; this opens up the possibility of developing simpler, smaller, low-power-consumption instruments for measuring low-kinetic-energy charged particles.

An experiment was performed to demonstrate the use of a δ-doped CCD to detect incident protons and measure their

kinetic energies. A δ-doped CCD with associated camera electronics was placed in a vacuum chamber, attached to a magnetically analyzed low-kinetic-energy proton-beam apparatus. The responses of the CCD were then measured at proton kinetic energies from 12 down to 1.25 keV. The CCD output signals were found to vary monotonically with proton kinetic energy throughout the energy range of the experiment.

This work was done Shouleh Nikzad, Blythe Elliott, Thomas Cunningham, Walter Proniewicz, D. R. Croley, G. B. Murphy, and Dale Winther of Caltech for **NASA's Jet Propulsion Laboratory**. *Further information is contained in a TSP [see page 1].*

In accordance with Public Law 96-517, the contractor has elected to retain title to this invention. Inquiries concerning rights for its commercial use should be addressed to

Technology Reporting Office
JPL
Mail Stop 122-116
4800 Oak Grove Drive
Pasadena, CA 91109
(818) 354-2240

Refer to NPO-20253, volume and number of this NASA Tech Briefs *issue, and the page number.*

Hardware, Techniques, and Processes

BLANK PAGE

GPS Drives Interactive Map Showing Position of Test Airplane

This system could augment, back up, or substitute for a radar-based system.

Dryden Flight Research Center, Edwards, California

An electronic system that comprises airborne and ground-based subsystems generates data for a global real-time interactive map (GRIM) that displays the current position and velocity of the NASA F-18 Systems Research Aircraft (SRA). This system utilizes the Global Positioning System (GPS) to determine the position and velocity of the aircraft; it serves as a prototype for the development of other, similar GPS-based systems that could be used for tracking and guidance of aircraft during flight research. Such GPS-based systems could be used to augment, back up, or substitute for radar-based tracking systems; indeed, as described below, the performance of the prototype GPS-based system has been compared with that of a radar-based tracking system in initial tests.

Located aboard the SRA, the prototype airborne subsystem includes a GPS receiver (see Figure 1). The output data from the GPS receiver are molded into a stream of telemetry data, which are transmitted from the SRA to a ground station on a pulse-code-modulated radio signal. The ground-based subsystem includes the GRIM display equipment, which resides in a control room at Dryden Flight Research Center. Previously, the GRIM was driven by data from a ground-based FPS-16 radar subsystem. The development of the present system included modification of the GRIM to make it possible to track the position and velocity of the SRA simultaneously by use of both radar and GPS information. The GRIM software was modified to display a triangle to represent the position based on radar data and a circle to represent the position based on GPS data (see Figure 2).

At the time of reporting the information for this article, the performances of the GRIM as driven by GPS and radar-based data had been evaluated and compared in more than ten research flights. Postflight analysis revealed that GPS data differed from radar data by the following:

Time lag	2 seconds
Horizontal position	GPS horizontal velocity × time lag
Vertical position (see figure)	±300 ft (±91 m)
Velocity	±20 ft/s (±6 m/s)

The system is not limited to a single aircraft. Multiple aircraft can be tracked on the GRIM, using GPS data only, radar data only, or both GPS and radar data. The capability to utilize GPS data is particularly advantageous in situations in which radar resources are insufficient or are unavailable because of competing priorities or schedules.

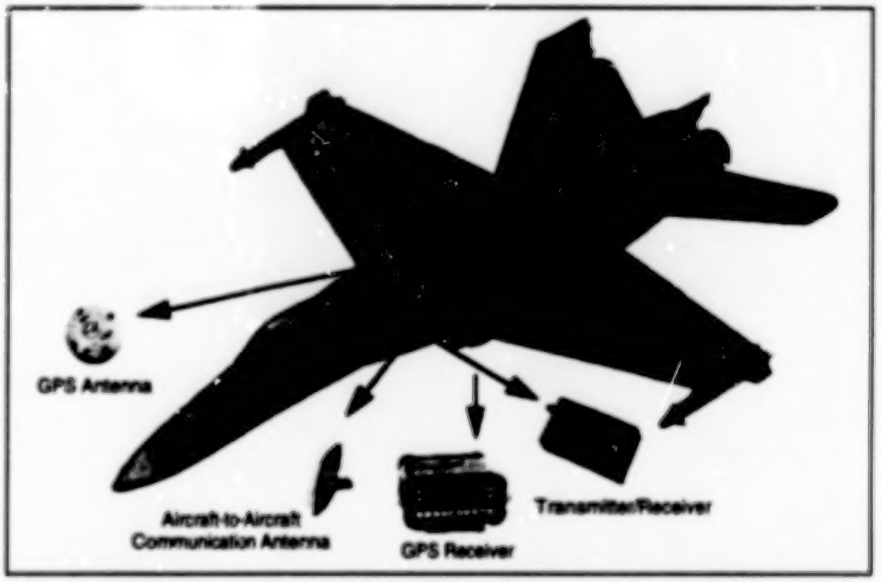

Figure 1. A GPS Receiver Mounted in the SRA tracks position and velocity in three dimensions in real time.

Figure 2. This GRIM Display, generated during a test flight, shows ground track and position as determined by GPS and radar.

This work was done by John McGrath; Ed Haering, Jr.; Harry Miller; Jack Tremp; Dave Webber; Glenn Bever; and Joe Collura of **Dryden Flight Research Center**; *Jules Ficke of SPARTA, Inc.; and George Aragon of OAO. Further information is contained in a TSP [see page 1].*

DRC-98-23

Terrestrial Portable Spacecraft-Mission-Support Stations

Augmented laptop computers would perform tracking, telemetry, command, monitoring, and control functions.

NASA's Jet Propulsion Laboratory, Pasadena, California

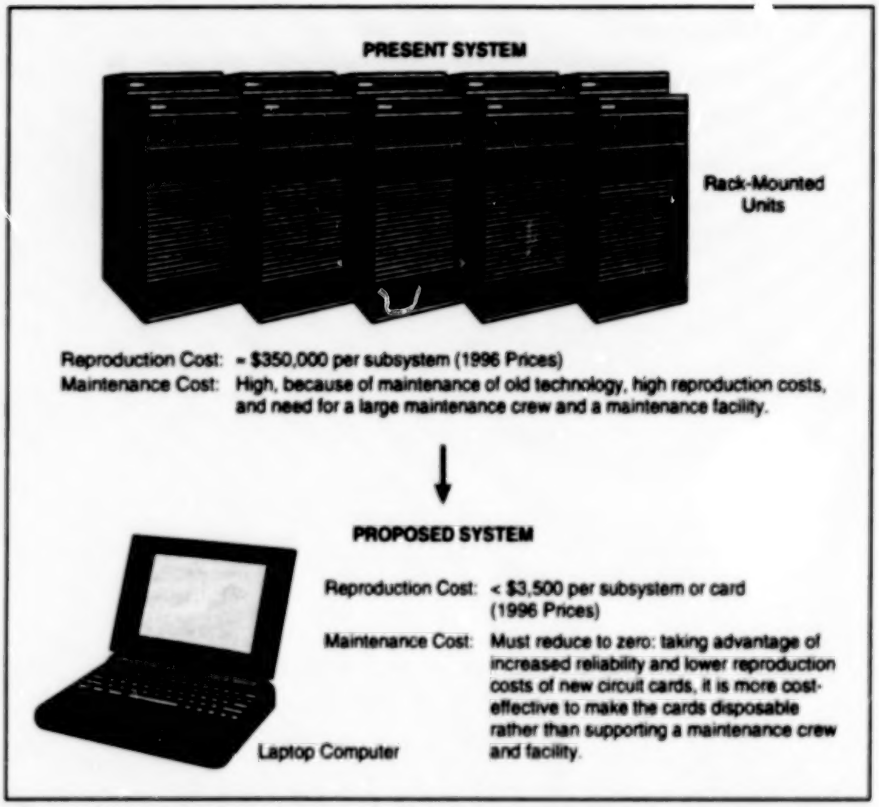

Mission-Support Electronic Systems Are Evolving from assemblies of expensive, obsolescent, rack-mounted units in central locations to cheaper, laptop-computer-based portable units.

A data-communication and -processing network of compact, laptop-computer-based portable stations communicating via the World Wide Web (WWW) has been proposed as a relatively inexpensive end-to-end ground support system for future spacecraft missions. At present, end-to-end ground support functions (receiving, tracking, telemetry, command, monitoring, and control) are distributed among several subsystems in rack-mounted chassis (see figure). Many of these subsystems have outdated designs that entail high reproduction, maintenance, and operational (labor) costs. The costs are even higher than they might otherwise be because some functions are duplicated by two independent systems at NASA's Jet Propulsion Laboratory: the Deep Space Communications Complex (DSCC) and the Advanced Multi-Mission Operation System (AMMOS). The AMMOS is an intermediate product of evolution toward the proposed system and is not an end-to-end system; in the AMMOS, some telemetric and interfacial functions are implemented in software on a laptop computer, at data rates that are too low for typical spacecraft missions.

In the proposed system, only the antenna subsystems, central command subsystems, receivers, transmitters, and data-storage or -buffering equipment would be retained at the DSCC. The other subsystems and the duplication between the DSCC and the AMMOS would be eliminated. Functions of tracking, ranging, command, monitoring and control, simulation and processing of telemetric data, central processing of data, and operation of the network would be performed by combinations of hardware and software in the portable stations.

To keep costs low, the portable stations would be made of commercial off-the-shelf products to the extent possible. To achieve the required data rates and promote modularity and interoperability, separate subsystem functions (e.g., telemetry, tracking, ranging, and command) would be implemented in hardware on separate circuit cards that conform to the Personal Computer Memory Card International Association (PCMIA) standard. The sizes of integrated circuits on the PCMIA cards could be reduced by use of multichip-module (MCM) packaging techniques.

A portable station could be operated at any suitable location in the world; for example, at the DSCC, aboard a vessel, at a field site on land, or in a researcher's office or laboratory at a university. The system would enable a scientist to perform multiple tasks simultaneously from such a location. For example, a scientist could perform a sea-floor geodesy experiment by use of the Global Positioning System while tracking a spacecraft and processing telemetric data. Inasmuch as only one operator (the scientist or an assistant) would be able to manage all of these tasks, the cost of operating the system would be less than that of operating the present system, which depends on multiple operators. The innovations discussed here are formulated concepts, and have not been fully reduced to practice.

This work was done by Barbara Lam of Caltech for **NASA's Jet Propulsion Laboratory**. *Further information is contained in a TSP [see page 1].*
NPO-20286

Training Neural Networks With Fewer Quantization Bits

Maximum synaptic weights are progressively reduced in the cascade back-propagation learning algorithm.

NASA's Jet Propulsion Laboratory, Pasadena, California

A method for reducing the number of bits of quantization of synaptic weights during training of an artificial neural network involves the use of the cascade back-propagation learning algorithm. The development of neural networks of adequate synaptic-weight resolution in very-large-scale integrated (VLSI) circuitry poses considerable problems of overall size, power

consumption, complexity, and connection density. Reduction of the required number of bits from the present typical value of 12 to a value as low as 5 could thus facilitate and accelerate development.

In this algorithm, neurons are added sequentially to a network, and gradient descent is used to permanently fix both the input and output synaptic weights connected to each added neuron before proceeding further. Each added neuron has synaptic connections to the inputs and to the output of every preceding neuron; thus, each added neuron implements a hidden neural layer. The addition of each successive neuron provides an opportunity to further reduce the mean squared error. Because the average number of connections to a neuron is small, learning is quite fast.

To adapt the cascade back-propagation algorithm to neural-network circuitry with limited dynamic range (equivalently, coarse weight resolution) in the synapses, one reduces the maximum synaptic conductances associated with neurons added later. This effectively reduces the sizes of synaptic-weight quantization steps, so that in the later stages, the desired synaptic-weight resolution is ultimately achieved and the learning objective approached as closely as required, without having to increase the number of bits (see figure).

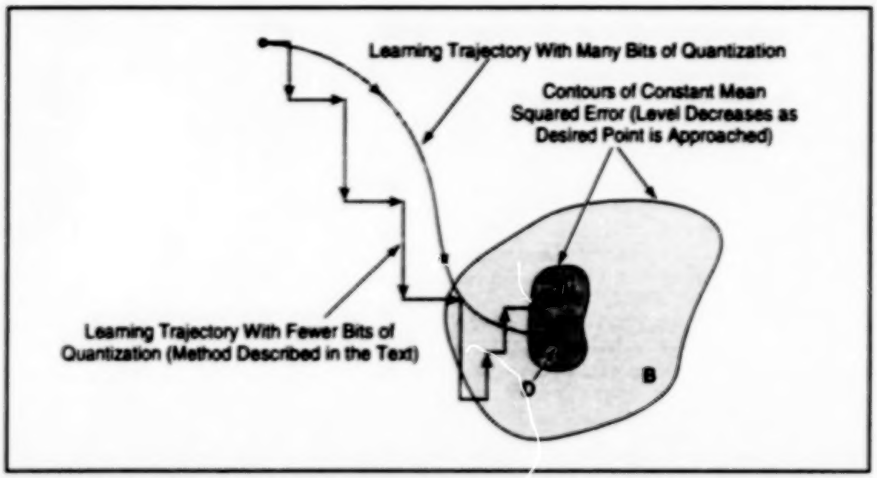

Learning Trajectories of a neural network are plotted symbolically in a plane, in which the two perpendicular axes represent the many synaptic-connection-weights. During learning according to the method of the text, the size of the steps is reduced when the trajectory reaches the contour at error level B. The size of the steps is further reduced upon reaching error level C. Learning is stopped upon reaching the contour at error level D.

Both simulations and tests with analog complementary metal oxide/semiconductor (CMOS) VLSI hardware have shown that by use of this method, neural networks can learn such difficult problems as 6-bit parity with synaptic quantizations as low as 5 bits, as opposed to the 8 to 16 bits required in the older error-back-propagation and cascade-correlation neural-network-learning algorithms.

This work was done by Tuan A. Duong of Caltech for **NASA's Jet Propulsion Laboratory**. *Further information is contained in a TSP [see page 1].*

NPO-19565

BLANK PAGE

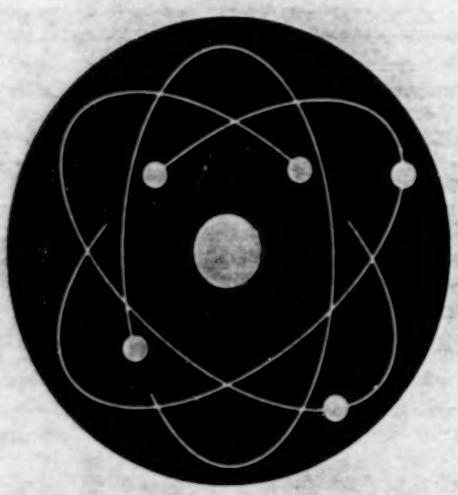

Physical Sciences

Hardware, Techniques, and Processes

BLANK PAGE

Heat Pipes for Temperature Control in Electronics

A 3-mm-diameter heat pipe keeps computer chips from blowing their cool.

Thermacore Inc., Lancaster, Pennsylvania

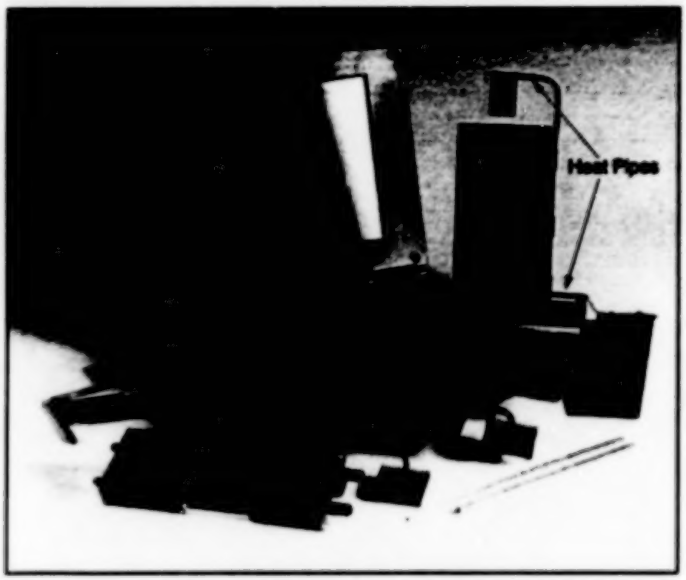

Figure 1. **Heat Pipes in Laptop Computers** help dissipate harmful concentrations of heat.

As electronic circuits become more densely packaged and higher in power, maintaining them within permissible temperature ranges becomes a major issue. This is especially true in the case of such portable devices as laptop computers, cellular telephones, and other hand-held units. Cooling by a conventional approach (for example, by use of a fan and a heat sink) ultimately reduces the useful battery power and the useful operating time of a portable device. Using its own funds, Thermacore Inc. employed knowledge gained from the Small Business Innovation Research (SBIR) program to develop a miniature high-performance heat pipe for use in cooling portable electronic devices.

A heat pipe is a sealed heat-transfer element. It makes use of two-phase heat transfer to carry heat at a small temperature drop from an input area, where a working fluid is evaporated, to an output area where the vapor is condensed, giving up its heat of vaporization. Capillary pumping in a porous wick structure returns the condensed liquid to be re-evaporated, thus making the heat pipe passive in the sense that no external power is needed for its operation.

In a laptop computer, a 3-mm-diameter heat pipe (see Figure 1) is used to spread the heat over a large area that is effectively cooled by natural convection. The ability of the 3-mm heat pipe to adequately transport the excess heat is due to a high-performance sintered powder metal wick structure that lines the interior wall. This wick structure also enables the heat pipe to work in any orientation. The heat-pipe pressure boundary and wick are made from copper, and water is the working fluid.

Given the high volume of computer manufacturing, the cost of heat pipes has been reduced significantly, quite often providing economical solutions to problems of cooling in many applications. Thermacore has used company funds to develop the fabrication process needed and to build the factory required for mass production of miniature heat pipes. Production rates have already exceeded 7,500 units per day.

The commercial success of the miniature heat pipes is spawning other advanced heat-pipe-based products. One such product entering the marketplace is the loop heat pipe (LHP) shown in Figure 2. The LHP includes a pair of narrow tubes (typically 3 mm in diameter), several meters long, along which heat can be transported while the tubes are in any orientation. The key to the performance of the LHP is the a small-pore (≤1 μm) powder metal wick structure in the evaporator section. This wick structure is typically made from nickel or stainless steel. The exterior pressure boundary material for of an LHP is made of stainless steel or aluminum.

Figure 2. This 4-Meter LHP delivered thermal power of 225 W against a 9-ft (2.7-m) adverse change in elevation.

LHPs were invented in the former Soviet Union in the early 1980s. Expertise in the design and fabrication of LHPs was brought to the United States by Thermacore Inc. in 1990. During the past several years, the ability to fabricate all aspects of LHPs was transferred to Thermacore Inc. and its sister company, Dynatherm Corp. This transfer created a United States supplier of LHPs and of expertise pertaining to LHPs.

A family of these devices has been produced to begin to address several applications, such as cooling of avionics in aircraft and missiles, aircraft anti-icing, regulation of temperatures in spacecraft, and solar heating to produce domestic hot water. Development of an LHP anti-icing system is being funded through the NASA SBIR program and monitored by NASA Lewis Research Center. LHPs will be used to passively transport engine waste heat forward to supply heat to critical surfaces to prevent ice formation. Because waste heat is used here, there is no power penalty and engine efficiency remains high. It is anticipated that an operational system will be demonstrated

on an unmanned aircraft in late 1998.

Loop heat pipes are also finding their way into applications on spacecraft. Dynatherm Corp. manufactures loop heat pipes for use on satellites. An American-made loop heat pipe was shown to operate successfully during a microgravitational flight experiment aboard the space shuttle (flight STS-87). Further advancements in LHPs are being funded by NASA Goddard Space Flight Center through the SBIR program.

LHPs are expected to be incorporated into rooftop heating units for producing domestic hot water. An LHP can accept solar energy on a roof and transport it passively to a water heater in the basement. Since the LHP subsystem of the hot-water system operates completely passively, an increase in system efficiency over that achieved without solar/LHP augmentation is anticipated.

This work was done by **Thermacore Inc.** *under NASA SBIR contracts monitored by* **NASA's Johnson Space Center, Goddard Space Flight Center,** *and* **Lewis Research Center.** *For more information, contact Mr. Nelson J. Gernert: telephone: (717) 569-6551; e-mail address: gernert@thermacore.com; Thermacore Inc., 780 Eden Road, Lancaster, PA 17601.*

Automatic Thermal Switches With No Moving Parts

The conductances of novel gas-gap thermal switches would increase with temperature.

NASA's Jet Propulsion Laboratory, Pasadena, California

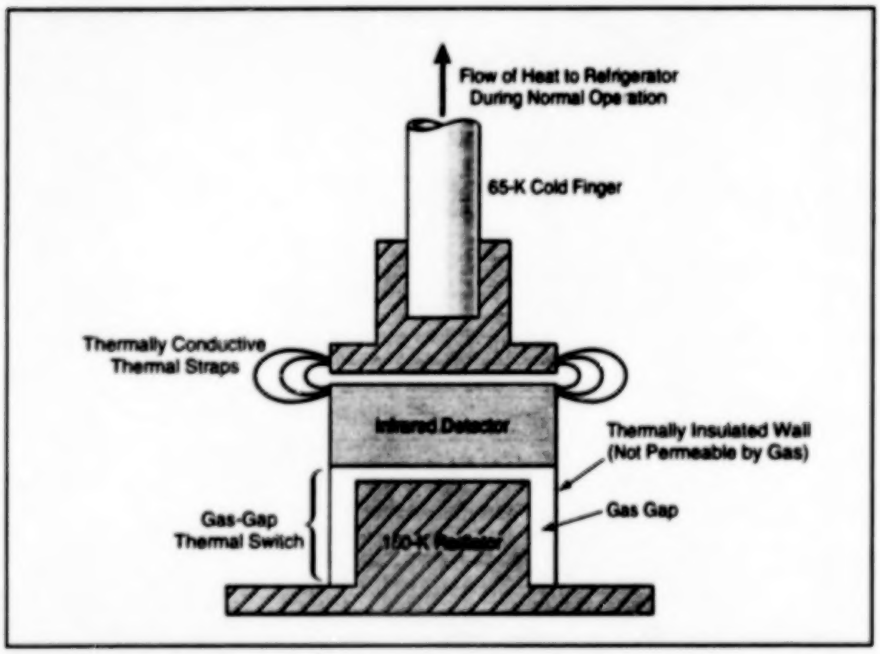

The Gap Would Be Effectively Empty and thus heat would not be conducted across the gap at an intended normal operating temperature of 65 K. At a higher temperature (150 K), the gap would be filled with carbon dioxide, rendering the gap thermally conductive, so that the infrared detector would be cooled by the radiator.

Quasi-thermostatic gas-gap thermal switches have been proposed. These switches would operate automatically, would contain no moving parts, would not require power supplies or controls, would not consume any materials, and would not create vibrations. The operation of a switch of this type would be based on the increase, with temperature, in the vapor pressure of a condensible fluid in a gap; the effective thermal conductance across the gap would increase with vapor pressure and thus with temperature. The design of the gap and the fluid would be chosen so that the thermal conductance across the gap would increase sharply with temperature in the desired switching temperature range.

In the original intended application, a thermal switch of this type would provide a thermal connection for backup radiative cooling of an infrared detector to a temperature of about 150 K in the event of failure of a refrigerator that would ordinarily provide cooling to 65 K (see figure). The fluid chosen for this application is carbon dioxide, which would condense in solid form on the infrared-detector side of the gap during normal operation at 65 K. Because the vapor pressure of carbon dioxide is only 10^{-14} torr ($\approx 10^{-12}$ Pa) at 65 K, the effective thermal conductance across the gap during normal operation would be negligible; that is, the radiator could be regarded as thermally disconnected from the infrared detector.

In the event of failure of the refrigerator, the temperature of the infrared detector would rise toward 150 K, causing some of the carbon dioxide to vaporize and fill the gap. At 150 K, the vapor pressure of carbon dioxide is 2.4 torr (320 Pa), and the effective thermal conductance across the gap would be about the same as though the carbon dioxide were at full atmospheric pressure and temperature. This level of thermal conductance would provide an effective thermal connection between the infrared detector and the radiator.

Upon resumption of normal operation, the vapor pressure of the carbon dioxide would decrease along with the temperature. At an intermediate temperature of 125 K, the vapor pressure of carbon dioxide is 1.5×10^{-2} torr (about 2 Pa), and the resulting effective thermal conductance across the gap would be of the order of 10^{-2} times that at 150 K; thus, the infrared detector would be effectively thermally disconnected from the radiator and could therefore be cooled more effectively by the refrigerator to the desired operating temperature of 65 K.

Gas-gap thermal switches based on the same principle could be designed for other temperature ranges, using other fluids. For example, water vapor could be used as the gap fluid for switching between active and passive means for cooling habitable spaces. For another example, mercury could be used as the gap fluid for switching at a temperature of about 450 K.

This work was done by Jack Jones and Dean Johnson of Caltech for **NASA's Jet Propulsion Laboratory.** *Further information is contained in a TSP [see page 1].*
NPO-19545

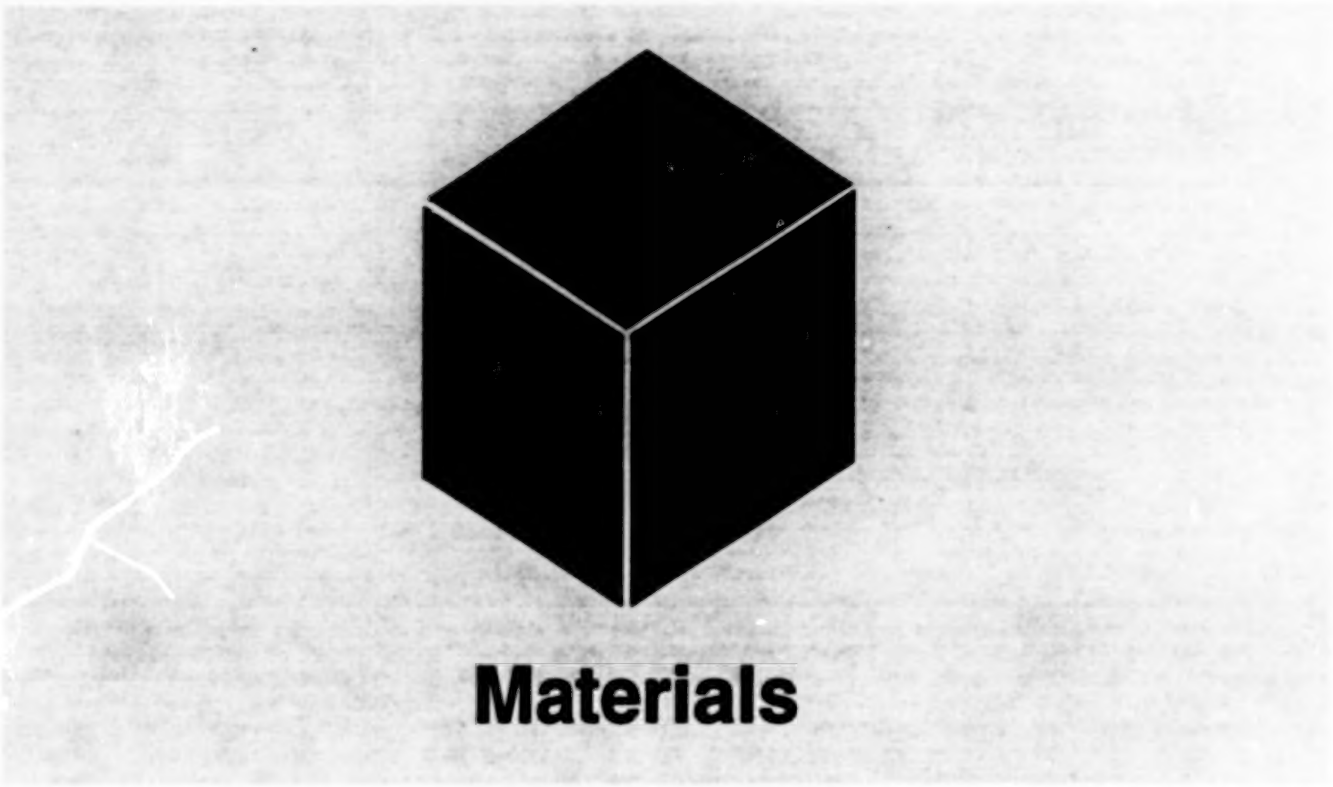

Materials

Hardware, Techniques, and Processes

BLANK PAGE

Software for Probabilistic Analysis of Composite Structures

An integrated software package exploits parallel processing to reduce computation time.

Lewis Research Center, Cleveland, Ohio

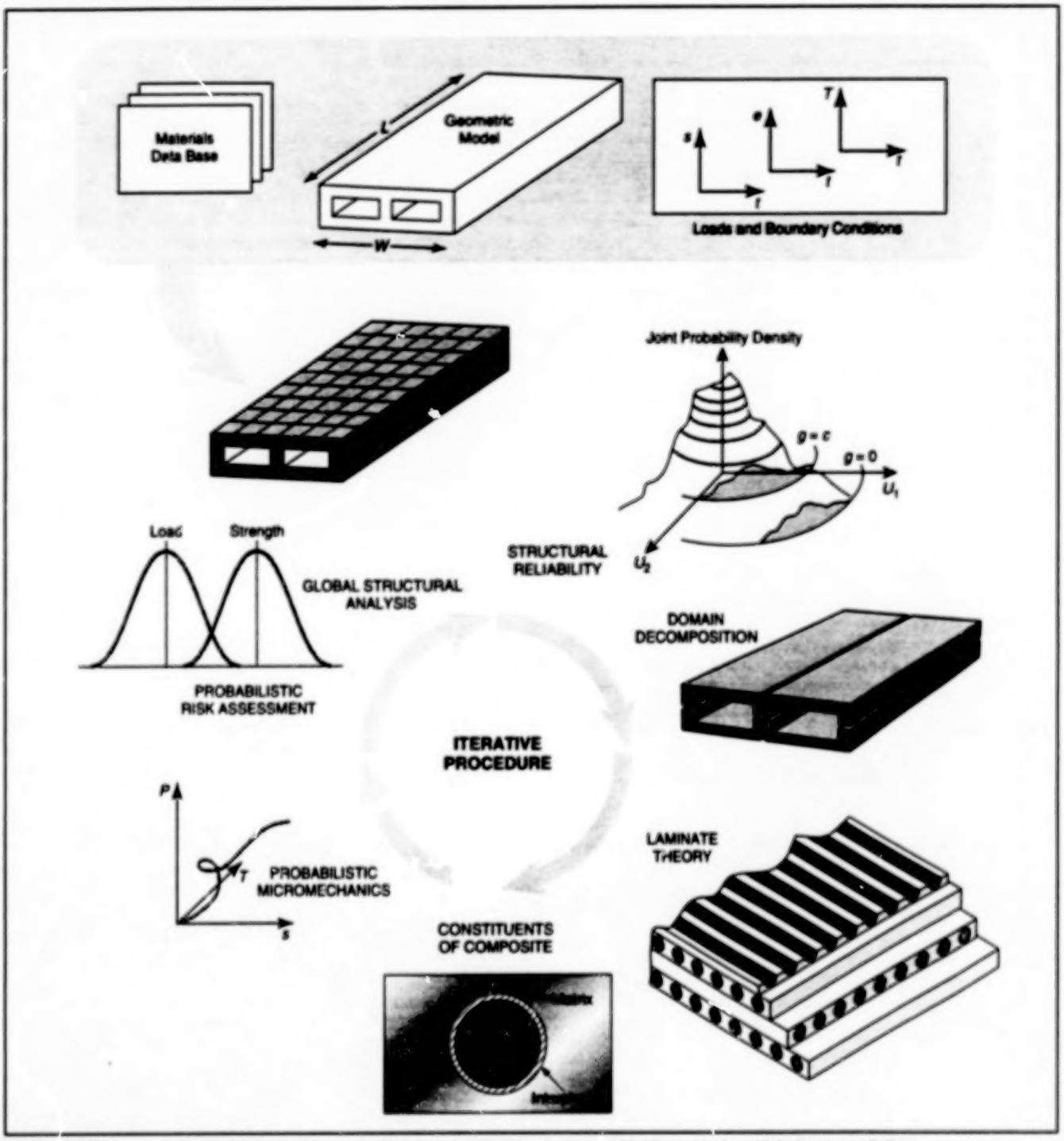

Analytical Components Are Integrated in an iterative computational procedure with hierarchical multiple-level parallelism.

GENOA is an advanced, completely integrated, hierarchical software package for computationally simulating the thermal and mechanical responses of high-temperature composite materials and of structures made of those materials. The development of GENOA was guided partly by the need for a computational tool that could accelerate the design process while making it possible to avoid designing structures to be unnecessarily heavy and expensive, as they can be when one follows a deterministic approach and uses simple safety factors to account for variability among structural components in the effort to design conservatively. GENOA implements a probabilistic approach in which design criteria and objectives are based on quantified reliability targets that are consistent with the inherently stochastic nature of the properties of materials and structures.

The probabilistic approach to design involves the use of the deterministic basic

equations of mechanics in a more-comprehensive analysis in which stochasticity is quantified by use of probability distributions. The methods used to simulate numerically the consequences of probability distributions include the Monte Carlo method and such algebraic methods as first-order reliability, second-order reliability, the mean-value method, or the response-surface method. Probabilistic methods provide measures of the variation of risks of failure with variations in design parameters and properties of materials, thereby making it possible to determine the robustness of a design. Realistic indications of the lifetimes of structures can be obtained by taking account of such phenomena as low cycle fatigue, cracking induced by flaws, yield and ultimate strengths, creep strength, the operational environment, and damage in service. The economic benefits of using probabilistic methods to design and analyze structures include (1) reduction of weights (and thus reduction of initial costs) of structures, (2) reduction of operating and service costs, (3) reduction failure rates, and (4) capability to generate predictable maintenance schedules.

GENOA provides computational integration and parallel processing for probabilistic mathematics and for mathematical models of composite materials and structures. Massively parallel processing enables GENOA to function in the face of the inherent complexities of high-temperature composite-material structures. Dynamic load-balancing optimization techniques are used in GENOA to minimize processing time. To perform a given analysis, GENOA takes about 1/20 of the processing time of a typical older serial-processing program developed for the same purpose.

GENOA features a highly modular architecture that makes it fast, accurate, and user-friendly. Hierarchical analytical components are implemented by software modules that contain highly specialized analysis codes (including nonlinear finite-element and micromechanical-analysis codes, for example). These components are integrated in a computational procedure that involves iteration between microscopic and macroscopic scales (see figure). The integration is effected by use of a graphical user interface (GUI) and an executive controller system (ECS). The menu-driven ECS connects the modules. The GUI provides a seamless transition from description of a problem through implementation of the solution process to post-processing graphical display of solution data. The value of integration cannot be over-emphasized: in GENOA, it is easy to import data from another structural-analysis or computer-aided-design program to describe a problem, whereas in most finite-element-analysis programs, such importation is difficult.

Analytical performance is enhanced by a capability to size adjacent problem domains dynamically to minimize processor waiting times. Central-processing-unit time is reduced and memory limitations are overcome by introduction of an effective optimized parallelization algorithm characterized by machine-independent multiple-instruction/multiple-data (MIMD), single-instruction/multiple-data (SIMD), and Open Software Foundation (OSF) types of computer architecture. Hierarchical stochastic simulation is performed to accommodate the numerous levels of uncertainty present in environmentally dependent properties of materials, enabling the user to identify quickly the most probable critical point of a design.

This work was done by Frank Abdi, Yvgeniy Mirvis, Jafar Hadian, and Kenneth J. Newell of Alpha STAR Corp. for **Lewis Research Center**. *Further information is contained in a TSP [see page 1].*

Inquiries concerning rights for the commercial use of this invention should be addressed to NASA Lewis Research Center, Commercial Technology Office, Attn: Tech Brief Patent Status, Mail Stop 7–3, 21000 Brookpark Road, Cleveland, Ohio 44135. Refer to LEW-16543.

Ion-Beam-Deposited DLC Coatings on Fine-Grain CVD Diamond

Friction and wear are reduced, relative to as-deposited CVD diamond.

Lewis Research Center, Cleveland, Ohio

Ion-beam-deposited surface layers of diamondlike carbon (DLC) on fine-grain chemical-vapor-deposited (CVD) diamond have been found to be effective in reducing friction and wear in a variety of environments, including ultrahigh vacuum. This discovery opens the possibility of taking fuller advantage of the properties of CVD diamond and DLC to manufacture protective coatings to provide solid lubrication and resistance to wear, erosion, and corrosion. Such coatings could be applied to surfaces of bearings, valves, cams, gears, and magnetic recording disks and tapes, for example. Notwithstanding the high costs of natural diamonds of gem quality, the costs of DLC and CVD diamond are similar to those of CVD and physical-vapor-deposited (PVD) carbide and nitride films. The one major disadvantage of DLC is its lack of resistance to high temperature; its use must be restricted to temperatures ≤250 °C in air and ≤350 °C in vacuum.

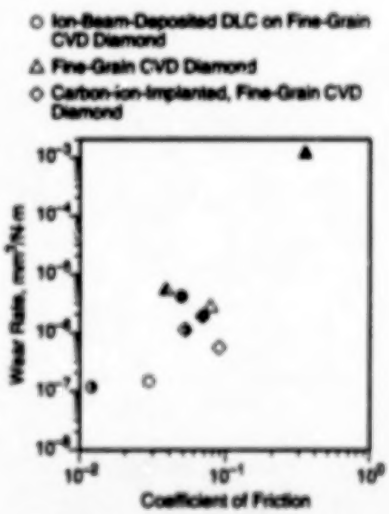

Wear Rates and Coefficients of Friction were determined in sliding-contact tests. Outline symbols indicate tests in humid air, half-darkened symbols indicate tests in dry nitrogen, and fully darkened symbols indicate tests in vacuum.

CVD diamond offers some solid lubrication and resistance to wear. However, friction and wear rates of as-deposited CVD diamond depend on the environment; in particular, they are greater in vacuum than in humid air or dry nitrogen. CVD diamond can be modified by carbon- or nitrogen-ion implantation to obtain an amorphous, nondiamond carbon surface layer that reduces friction and wear regardless of the environment. However, the surface layer is usually ≤0.5 μm thick; consequently, endurance is limited in the sense that use must typically be limited to light-load and/or short-term operations. In contrast, DLC films can be deposited to thicknesses as great as 5 μm, with concomitant potential for increasing endurance.

The wear-reducing and self-lubricating properties of specimens of ion-beam-

deposited DLC on fine-grain CVD diamond were investigated in a series of experiments. For comparison, specimens of ion-beam-deposited DLC on silicon and specimens of both as-deposited and carbon-ion-implanted fine-grain CVD were also included in the experiments. The specimens were fabricated on flat disk silicon substrates, then coefficients of friction were measured while the specimens were rotated in sliding contact with CVD-diamond-tipped hemispherical pins.

The sliding-contact tests were performed in humid air, dry nitrogen, and vacuum. Surface profilometry was performed to characterize surface features and determine surface roughnesses and depths of wear. The results of the sliding-contact tests (summarized in the figure) indicate that ion-beam-deposited DLC can effect significant reductions in the friction and wear of fine-grain CVD diamond.

This work was done by Kazuhisa Miyoshi of **Lewis Research Center** *and Richard C. Wu and William C. Lanter of K Systems Corp. Further information is contained in a TSP [see page 1].*

Inquiries concerning rights for the commercial use of this invention should be addressed to NASA Lewis Research Center, Commercial Technology Office, Attn: Tech Brief Patent Status, Mail Stop 7–3, 21000 Brookpark Road, Cleveland, Ohio 44135. Refer to LEW-16564.

Matrix and Coating Polymers for Composite LOX Containers

These polymers offer a combination of desirable properties.

Marshall Space Flight Center, Alabama

Two poly(arylene ether phosphine oxide)s (PAEPOs) have been found to be suitable as matrix and coating materials for composite-material (matrix/fiber) tanks and pipes that contain liquid oxygen (LOX). One of these PAEPOs is denoted by the trade name "Triton Oxygen Resistant" (TOR); this is a clear, yellowish material with the structural formula shown in the figure. The other PAEPO is a clear, colorless material called "colorless oxygen resistant" (COR).

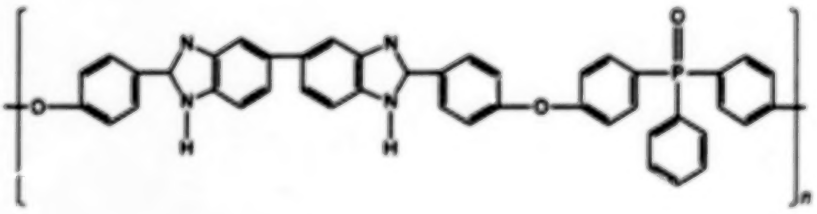

A Member of the PAEPO Family of Polymers, the polymer represented by this structural formula is a clear, yellowish material that is compatible with liquid oxygen.

These polymers exhibit properties that make them attractive for incorporation into composite-material LOX containers:

- They are physically and chemically compatible with LOX.
- They are compatible with the other component materials (toughened epoxies and graphite fibers) of composite-material LOX containers.
- They are amenable to processing by techniques used commonly in the fabrication of composite-material structures.

Some other commercially available polymers are compatible with liquid oxygen, but the use of them is inhibited, variously, by poor adhesion to other component materials, difficulties in processing, and/or the need to process them at temperatures high enough to damage other component materials.

These PAEPOs in film form have been shown to be highly compatible with LOX. The films have passed the Marshall Space Flight Center LOX mechanical-impact-sensitivity test at the maximum required energy level of 72 ft-lb (98 J). The PAEPOs are soluble in a number of polar solvents and can therefore be applied from solution onto complexly shaped surfaces with relative ease; for example, by dip coating or brushing. The PAEPO films can be made very thin if necessary, and they adhere well to composites made of other component materials.

These PAEPOs can also be used as matrix materials, along with graphite-fiber reinforcements, in prepregs and in composites made from prepregs by standard thermoplastic-matrix-composite consolidation techniques: A composite panel can be laid up by stacking multiple prepreg plies; the layup is then vacuum bagged and consolidated in a hot press or autoclave. However, like composites made with other matrix materials, composites made with these polymers fall shy of the neat polymer films in LOX testing. The reason for this behavior and what (if anything) can be done about it will be addressed in subsequent development work.

Although a PAEPO film can be applied to a previously cured epoxy-matrix/graphite fiber structure, the most unique and promising way of coating such a structure with a PAEPO film is to make the film become intimately bonded with the underlying composite by use of the composite cocure process. In this approach, a thin film of the PAEPO is applied on one side of a epoxy/graphite prepreg layup prior to curing. Then as the layup is cured to the finished composite, the film forms a strong bond with the epoxy matrix. This process offers two advantages: (1) it is solventless and (2) it results in an excellent bond.

This work was done by Marvin A. Gulles and Ross Haghighat of Triton Systems, Inc., for **Marshall Space Flight Center**. *Further information is contained in a TSP [see page 1].*
MFS-26541

BLANK PAGE

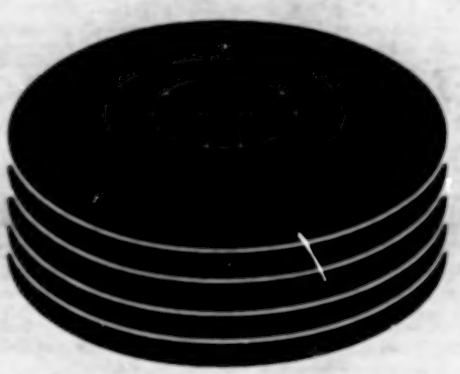

Computer Programs

Mechanics

BLANK PAGE

Computer Programs

These programs may be obtained from COSMIC. Please contact

COSMIC®
Computer Services Annex
University of Georgia
Athens, GA 30602
Telephone No. (404) 542-3265.

Mechanics

Program Performs High-Precision Spacecraft-Constellation Navigation

The *M*ultiple *I*nterferometric *R*anging *A*nalysis Using GPS *E*nsemble (MIRAGE) computer program processes spacecraft-tracking data to determine orbits of single satellites, or of multiple satellites with intersatellite tracking, to within position errors as small as a few centimeters (see figure). MIRAGE also targets spacecraft maneuvers (changes of velocity) to precision higher than that achievable by current spacecraft hardware. Tracking data that MIRAGE can utilize include Global Positioning System (GPS) pseudorange and phase, data from general range and Doppler measurements, angles, data from optical measurements, and data from very-long-baseline interferometry (VLBI). The modular program structure enables addition of other tracking data types for specific user spacecraft.

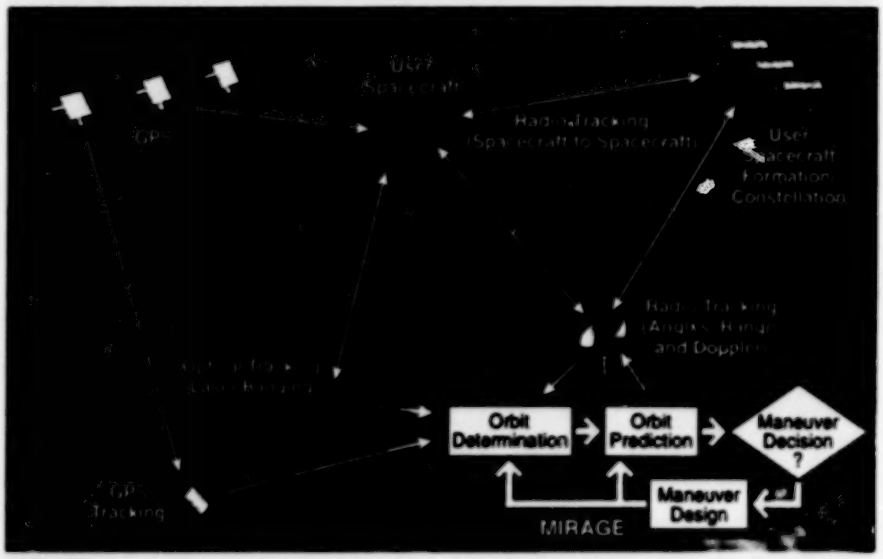

MIRAGE serves as a navigation system for multiple Earth-orbiting spacecraft. This diagram summarizes its functions.

MIRAGE implements a variety of geometrical and dynamical models that the user can control. A pseudo-epoch-state filter in MIRAGE smooths over data arcs selectable by the user, yielding robust solutions in the presence of bad tracking data and modeling errors. Operation is simplified through a system of interdependent and automated Unix and Perl scripts or through interactive X-Window menu-driven software wrappers. MIRAGE could be particularly useful for navigating multiple satellites to maintain them in a constellation for global telecommunications.

This program was written by Bobby G. Williams, Peter J. Wolff, Rick F. Sunseri, Theodore R. Drain, James B. Collier, Tseng-Chan Wang, and Joseph R. Guinn of Caltech for **NASA's Jet Propulsion Laboratory**. *Further information is contained in a TSP [see page 1].*
NPO-20287

Software for Navigation of a Spacecraft Flying in Formation

The Spacecraft Autonomous Navigation System using GPS for Earth Orbiters (SANS-GEO) computer program is designed to perform the navigation calculations that will enable the New Millennium Program's Earth Orbiter-1 (EO-1) spacecraft to fly in formation with the Landsat-7 (LS-7) satellite in orbit around the Earth. Scheduled to be launched in May 1999, the EO-1 will be required to follow 450±50 km behind the LS-7, and to keep its ground track within 3 km of the LS-7 ground track. Using data from an onboard Global Positioning System (GPS) receiver and empirical (purely kinematic) GPS navigation algorithms, SANS-GEO would compute parameters of the EO-1 orbit; these parameters would include rates of atmospheric-drag-induced decay. SANS-GEO would then utilize these parameters, along with the corresponding parameters and with maneuver plans generated remotely for the LS-7, to determine EO-1 velocity-change maneuvers needed to satisfy absolute orbital constraints (e.g., ground-track-repeat requirements) and/or

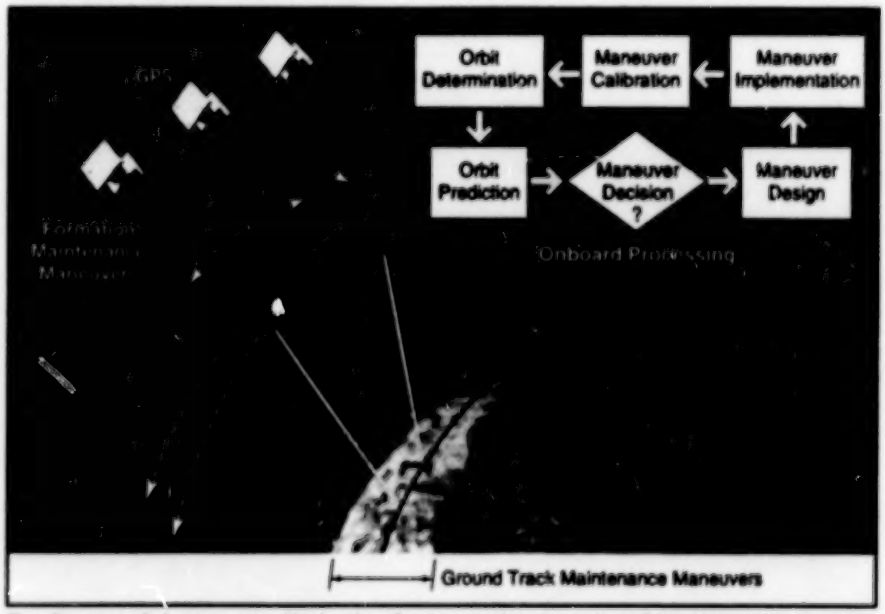

The Spacecraft Autonomous Navigation System depicts the extent of the onboard processing.

relative orbital constraints (formation-flying requirements). The computed velocity-change maneuvers would be converted into commands for the EO-1 attitude-control system and thrusters.

This program was written by Joseph Guinn of Caltech for **NASA's Jet Propulsion Laboratory**. *Further information is contained in a TSP [see page 1].*

This software is available for commercial licensing. Please contact Don Hart of the California Institute of Technology at (818) 393-3425. Refer to NPO-20190.

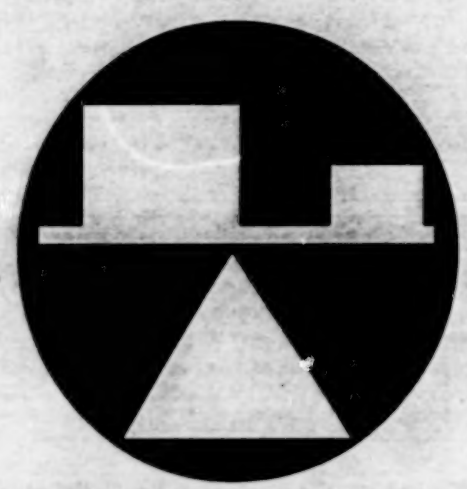

Mechanics

Hardware, Techniques, and Processes

BLANK PAGE

Finite-Element Model of Piezoelectric and Thermal Effects

Layerwise finite elements enable modeling of responses of "smart" piezoelectric composite structures.

Lewis Research Center, Cleveland, Ohio

A mathematical model that includes layerwise finite elements has been developed for use in numerical simulation of the coupled electrical, mechanical, and thermal responses of composite plate structures that incorporate piezoelectric sensors and actuators. Typically, the sensors and actuators in these so-called "smart" structures consist mainly of patches or layers of piezoceramic material. These "smart" structures can be used to sense and/or induce stresses, strains, and/or displacements in themselves or in larger structures of which they are parts. In one important class of potential applications that is particularly relevant to the present mathematical model, the piezoelectric actuators would be used to counteract thermal distortions.

The mathematical derivation of the model begins with the representation of coupled mechanical, electrical, and thermal responses at the material level by a set of simultaneous equations that include (1) the equation for mechanical equilibrium in the presence of stress; (2) Maxwell's equation for the conservation of electric displacements; and (3) the constitutive equations that express the relationships among strain, electric field, and temperature in a thermopiezoelectric material. The mechanical displacement, electric potential, and temperature are assumed to be fields that are layerwise continuous through the thickness of a given laminate or plate structure. This assumption provides the capability to capture locally induced piezoelectric effects, leading to increased accuracy in prediction of stresses, especially in a laminate that is thick and/or that exhibits strong through-the-thickness thermal and elastic inhomogeneities.

The layerwise formulation leads to a corresponding finite-element formulation for a bilinear plate element. The finite-element equations can be put into a compact matrix form, with the electric potential partitioned into active (applied) and sensory components. The advantage of this form is that the unknown variables (displacements and sensory electric potentials) appear on the left side, while the known quantities (mechanical loads, thermal loads, electric charges, and applied voltages) appear on the right side of the equation. The partitioned equations can be uncoupled into an independent equation for mechanical displacements and another independent equation for sensory electric potentials.

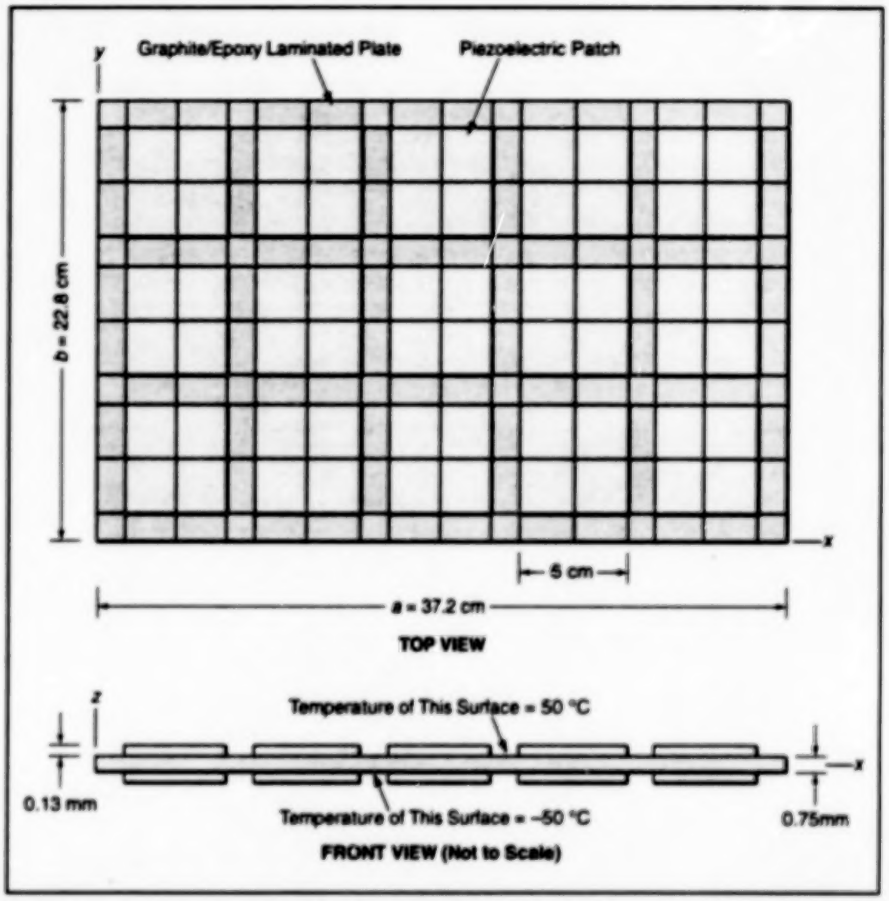

Figure 1. This Graphite/Epoxy Plate With Piezoceramic Patches on its upper and lower surfaces was considered to be simply supported at its right and left edges, and subject to a thermal gradient through its thickness.

In a test case, the model was applied in a simulation of the behavior of a thermally loaded [0°/±45°] graphite/epoxy laminated plate with a total of 30 piezoceramic patches mounted in symmetrical patterns on the top and bottom surfaces. The plate (see Figure 1) was considered to be simply supported along its *y* edges, and to be subjected to a thermal gradient from a temperature of 50 °C at its top surface to –50 °C at its bottom surface. The model was used to calculate the distortion caused by the thermal gradient alone, plus the combined effects of the thermal gradient and piezoelectric actuation. The numerical results, plotted in Figure 2, indicate that application of equal potentials of 70 V to the upper and lower piezoelectric patches counteracts the thermal distortion to such an extent as to reduce the center-line deflection to near zero.

This work was done by Ho-Jun Lee of **Lewis Research Center** *and Dimitrios A. Saravanos of Ohio Aerospace Institute. Further information is contained in a TSP [see page 1].*

Inquiries concerning rights for the commercial use of this invention should be addressed to NASA Lewis Research Center, Commercial Technology Office, Attn: Tech Brief Patent Status, Mail Stop 7–3, 21000 Brookpark Road, Cleveland, Ohio 44135. Refer to LEW-16537.

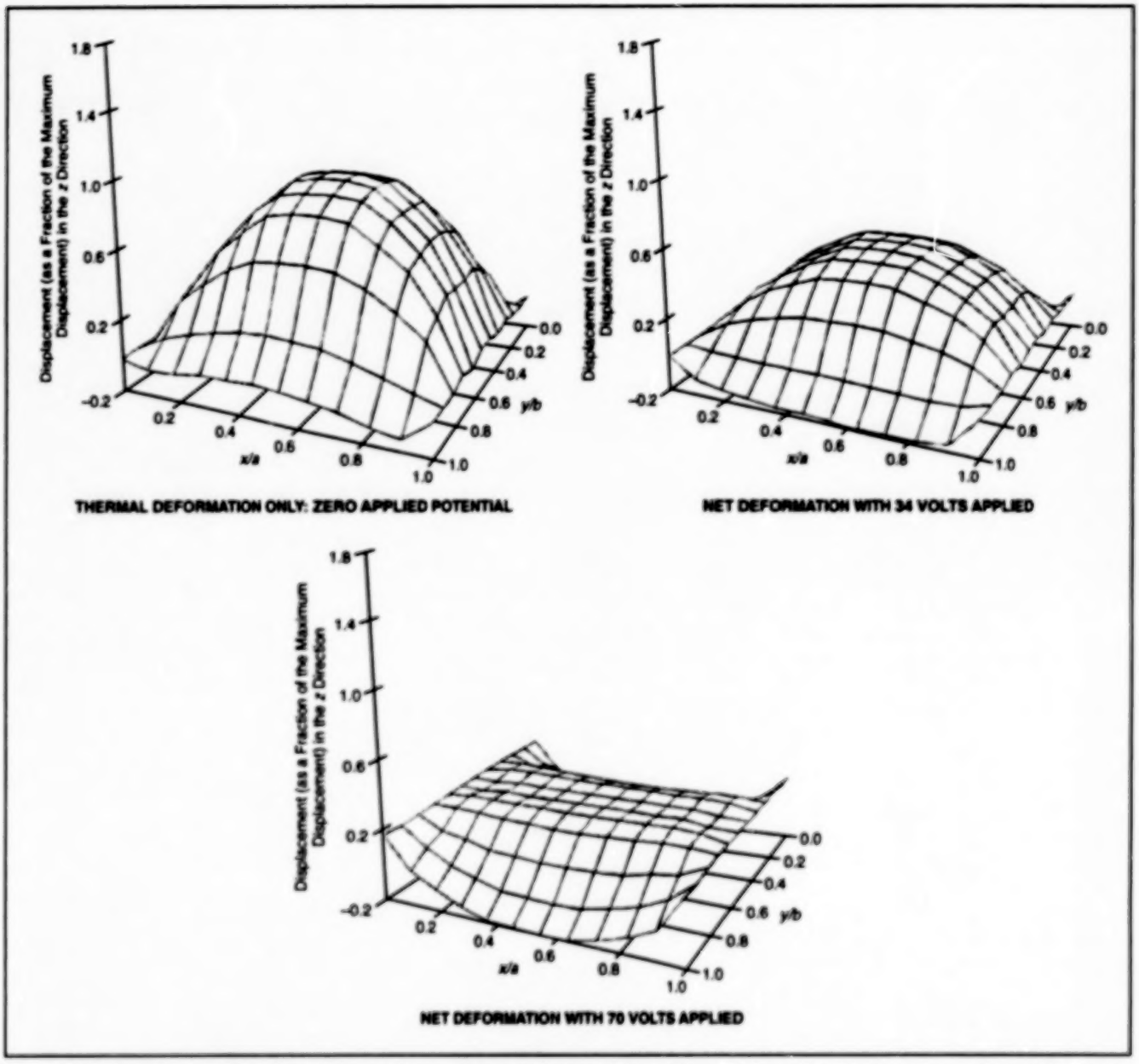

Figure 2. **Displacements of the Plate** of Figure 1 were computed by use of the mathematical model to illustrate the capability of the model and the use of piezoelectric actuation in a "smart" structure to counteract thermal distortion.

Passive Capture Joint With Three Degrees of Freedom

New joint allows quick connection between any two structural elements where rotation in all three axes is desired.

Marshall Space Flight Center, Alabama

A new joint, proposed for use on an attachable debris shield for the international Space Station Service Module, has potential for commercial use in situations where hardware must be assembled and disassembled on a regular basis.

This joint can be useful in a variety of applications, including replacing the joints commonly used on trailer-hitch tongues and temporary structures, such as crane booms and rigging. Other uses for this joint include assembly of structures where simple rapid deployment is essential, such as in space, undersea, and in military structures.

This new joint allows for quick connection between any two structural elements where it is desirable to have rotation in all three axes. The joint can be fastened by moving the two halves into position. The joint is then connected by inserting the ball into the bore of the base. When the joint ball is fully inserted, the joint will lock with full strength. Release of this joint involves only a simple movement and rotation of one part. The joint can then be easily separated.

Most passive capture devices allow only axial rotation when fastened — if any movement is allowed at all. Manually- or power-actuated active joints require an additional action, or power and control signal, as well as a more complex mechanism.

The design for this new joint is relatively simple. It consists of two halves, a ball

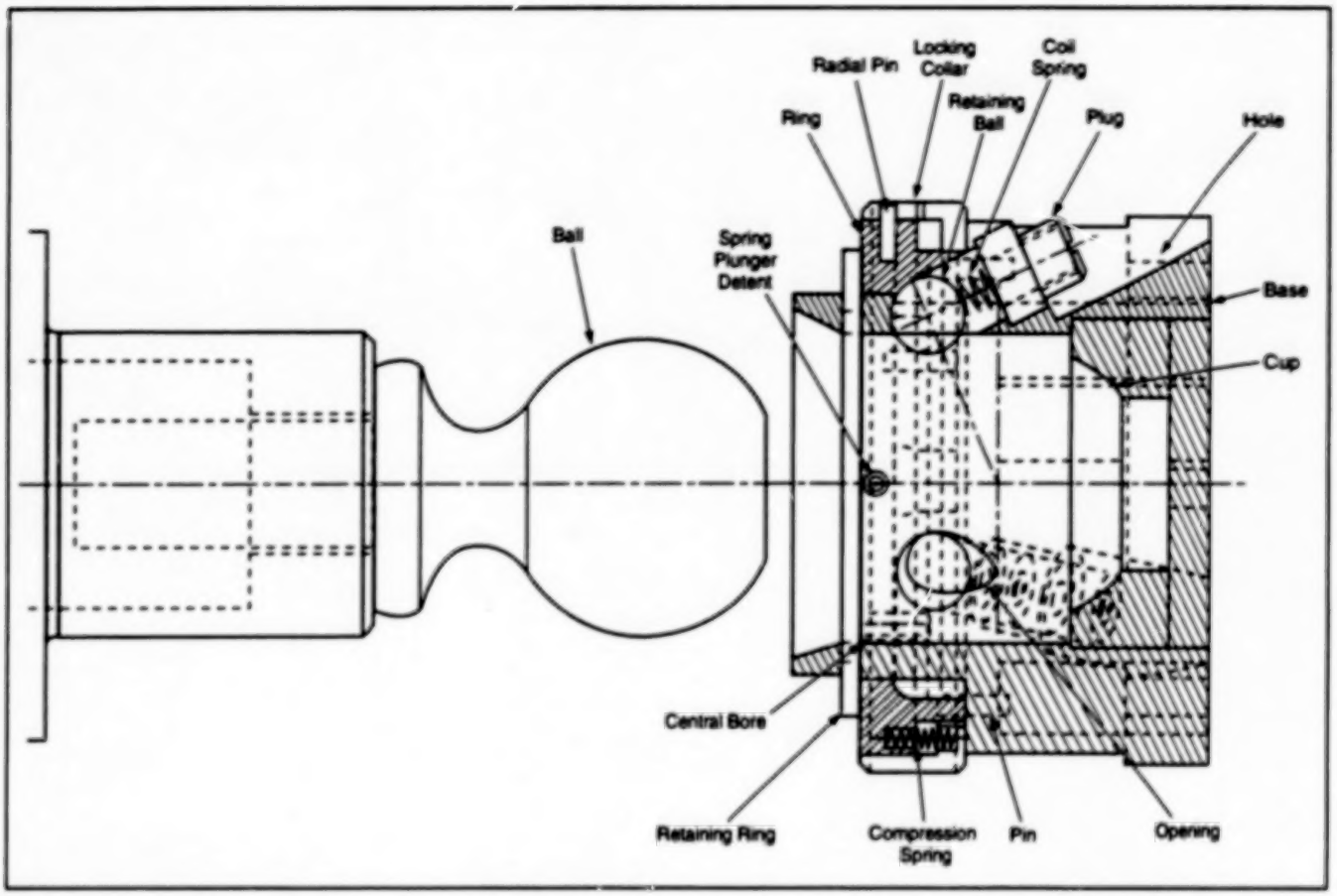

The three-degrees-of-freedom capability of the **Passive Capture Joint** provides for quick connect and disconnect operations.

mounted on a stem (such as those used on a common trailer-hitch ball) and a socket. The socket contains all the moving parts and is the important part of this invention. The socket also has a base, which contains a large central cylindrical bore ending in a spherical cup.

This work was done by Bruce Weddendorf and Richard A. Cloyd of the **Marshall Space Flight Center**. *Further information is contained in a TSP [see page 1].*

Inquiries concerning rights for the commercial use of this invention should be addressed to the Patent Counsel, Marshall Space Flight Center [see page 1]. Refer to MFS-31146.

Emergency-Shutoff Valves Would Be Triggered by Accelerations

These valves could stop flows of liquids in earthquakes, explosions, and vehicular impacts.

NASA's Jet Propulsion Laboratory, Pasadena, California

Automatic valves have been proposed for shutting off flows of liquids when abnormally large accelerations occur. These valves could be used, for example, to prevent outflows of flammable, valuable, or toxic liquids from pipelines that have been struck by vehicles or that have become involved in earthquakes or explosions. Actuation of the proposed valves would not depend on sources of electrical or fluid power, which would likely be unavailable during the emergencies in which the valves would be needed. Actuation would not even depend on pressurization of the liquids to be contained. Instead, the valves would operate similarly to spring-actuated rat traps, and like such traps, the valves could also be opened or closed manually.

The shaft for opening and closing a typical proposed valve would be connected to a lever, which would be spring-loaded toward the closed position. The lever would be turned against the spring load to open the valve (see figure). At the fully open position, an approximately hemispherical tip on the lever would face a similar tip on a stationary cocking stop. An inertial triggering object (in a ball in the case illustrated) would be placed between the tips to keep the valve open. The ball would be held in place by spring force and associated friction. A sufficiently large acceleration would dislodge the ball, allowing the spring to turn the lever and shaft to the closed position. The triggering sensitivity would vary inversely with the inertial force needed to overcome friction to slide the ball out from between the tips; this force would depend on the choice of the materials, sizes, shapes, and surface finishes of the ball and tips.

This work was done by Andrew D. Morrison of Caltech for **NASA's Jet Propulsion Laboratory**. *Further information is contained in a TSP [see page 1].*
NPO-20114

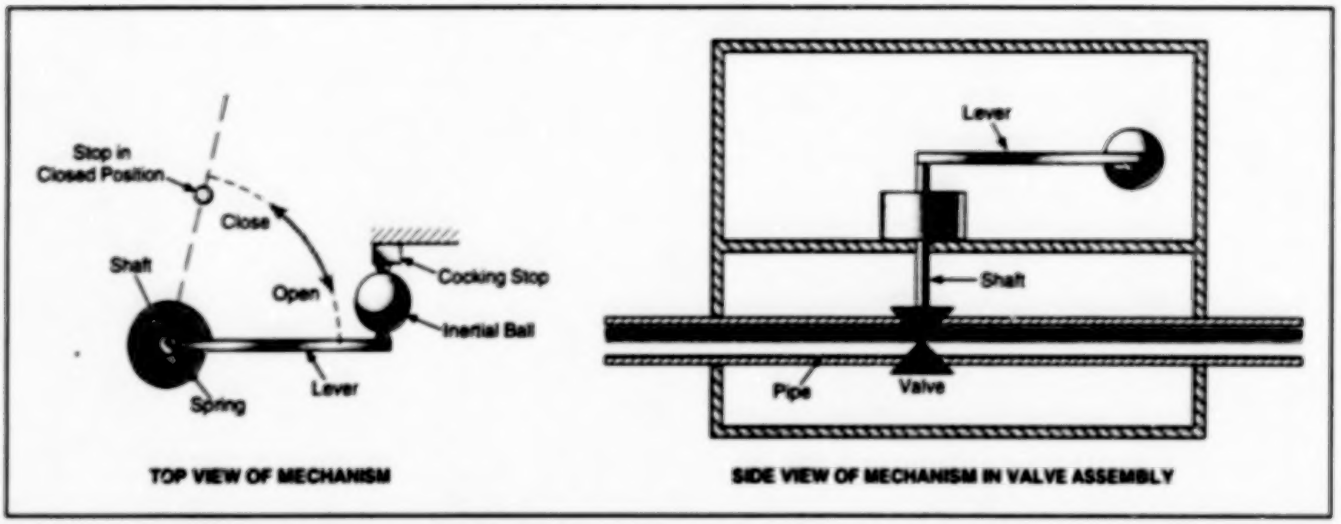

Acceleration Would Trigger the mechanism by dislodging the ball from between the tips on the lever and the cocking stop. The spring would then act on the lever, turning the shaft to close the valve.

Machinery

Hardware, Techniques, and Processes

BLANK PAGE

Simulations in Support of Towed Flight Demonstration

Two independent simulations run simultaneously to study towed-aircraft response before flight.

Dryden Flight Research Center, Edwards, California

The Eclipse flight project was established to demonstrate a reusable-launch-vehicle concept developed by Kelly Space and Technology, Inc. An F-106 delta-wing aircraft was chosen as the towed vehicle, and a C-141A transport-type airplane was selected for the towing vehicle. These airplanes are shown in Figure 1. Dryden Flight Research Center was the test organization with responsibility for safety of flight on the Eclipse project.

To enhance safety of flight, simulations of the two airplanes were implemented along with a simple mathematical model of a tow rope. A computational simulation of an F-106 airplane had been implemented at Langley Research Center to support some vortex-flow flight experiments, and this simulation was revived at Dryden. The C-141 simulation was adapted from an existing B-720 simulation at Dryden by replacing the mathematical model of the aerodynamics of the B-720 airplane with linear aerodynamic coefficients based on the performance of the C-141 airplane. The mathematical model of the B-720 engine was modified with a thrust multiplier to match the C-141 static sea-level thrust. In addition, the simulation was updated with C-141 weight, inertia, and center-of-gravity data. Existing simulation cockpits were used without modification.

The tow-rope model assumes that the tow rope lies on straight line between the two airplanes. On the basis of results from laboratory tests, the rope tension was modeled as quadratic in elongation and linear in elongation rate. This tow-rope model was verified initially by implementing it in a glider simulation and having a glider pilot subjectively evaluate the performance.

Initial studies were performed with the F-106 simulation alone. In these studies, it was assumed that the C-141 airplane was a point mass that would be unaffected by the forces on the tow rope. C-141 takeoff trajectories were generated and recorded in the C-141 simulation. These trajectories were played back in the F-106 simulation to study the takeoff performance of the towed F-106. This first cut showed some interesting results. The F-106 performance on tow was quite different from that of a sailplane. There appeared to be a lower and an upper bound on the tow angle between the two airplanes. Flight beyond these bounds would cause divergent pitch and sometimes roll oscillations. Fortunately, the oscillation amplitude would increase slowly enough that the pilot was able to recognize the problem and correct for it by flying back within the bounds. The simulation was already providing important information to the flight-test team.

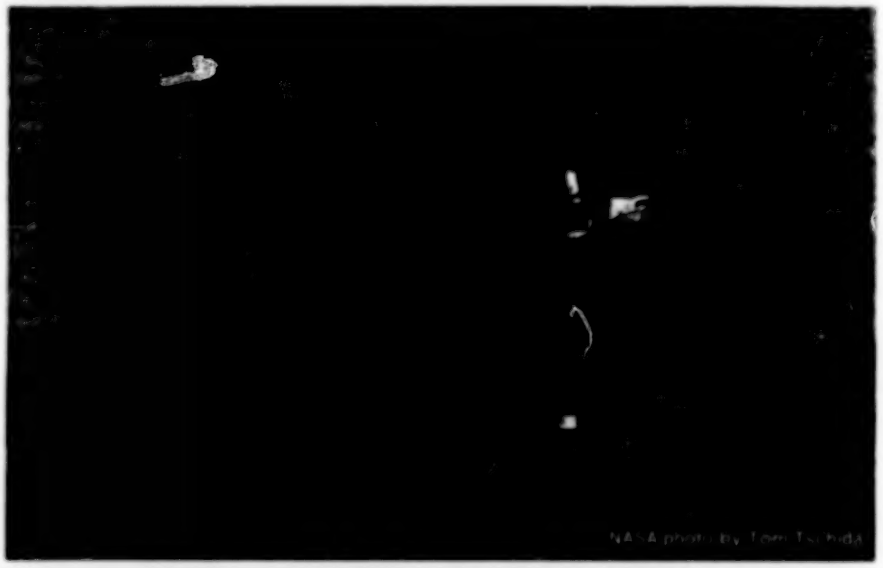

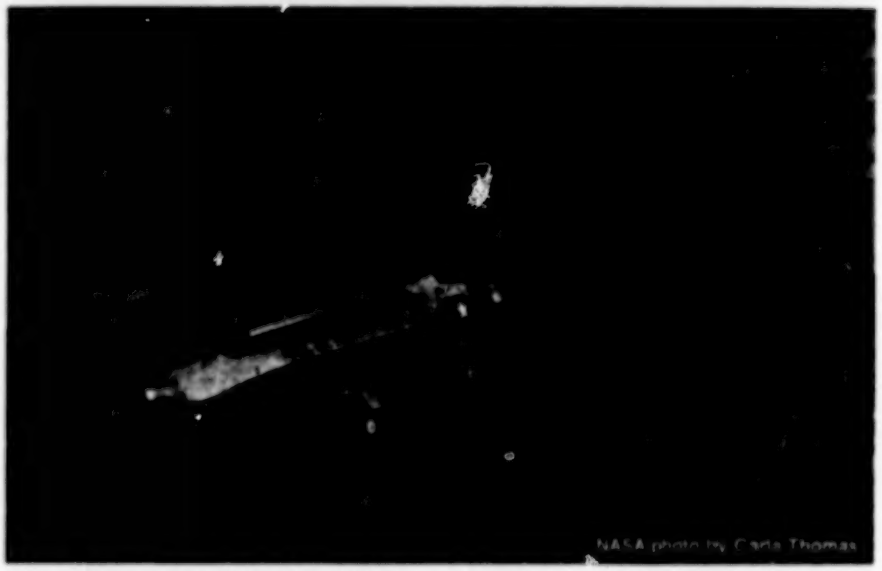

Figure 1. These Aircraft Were Used To Demonstrate the concept of towing a reusable aerospace vehicle to launch altitude.

To make the simulation study more realistic, it was decided that simulations of both airplanes should be performed simultaneously. To do this, it was necessary to link two independent six-degree-of-freedom (6-DOF) simulations — essentially creating a 12-DOF simulation. Although this seemed challenging at first, it turned out to be quite simple. The two simulation computers were linked with a fiber-optic reflective memory interface; this linkage enabled the sharing of airplane positions, velocities, and tow-rope forces between the two simulations.

To obtain consistent results, it was decided to synchronize the two simulations. The frame rates of both simulations were increased to 100 Hz, and flags in shared memory were created to enable the simulations to synchronize by polling. The interrupt driver in the F-106 simulation was used to generate the 100-Hz frame pulse, and the C-141 simulation simply waited for the F-106 simulation to indicate that a new frame should be started. The synchronization scheme is shown in Figure 2.

The results of the linked simulations con-

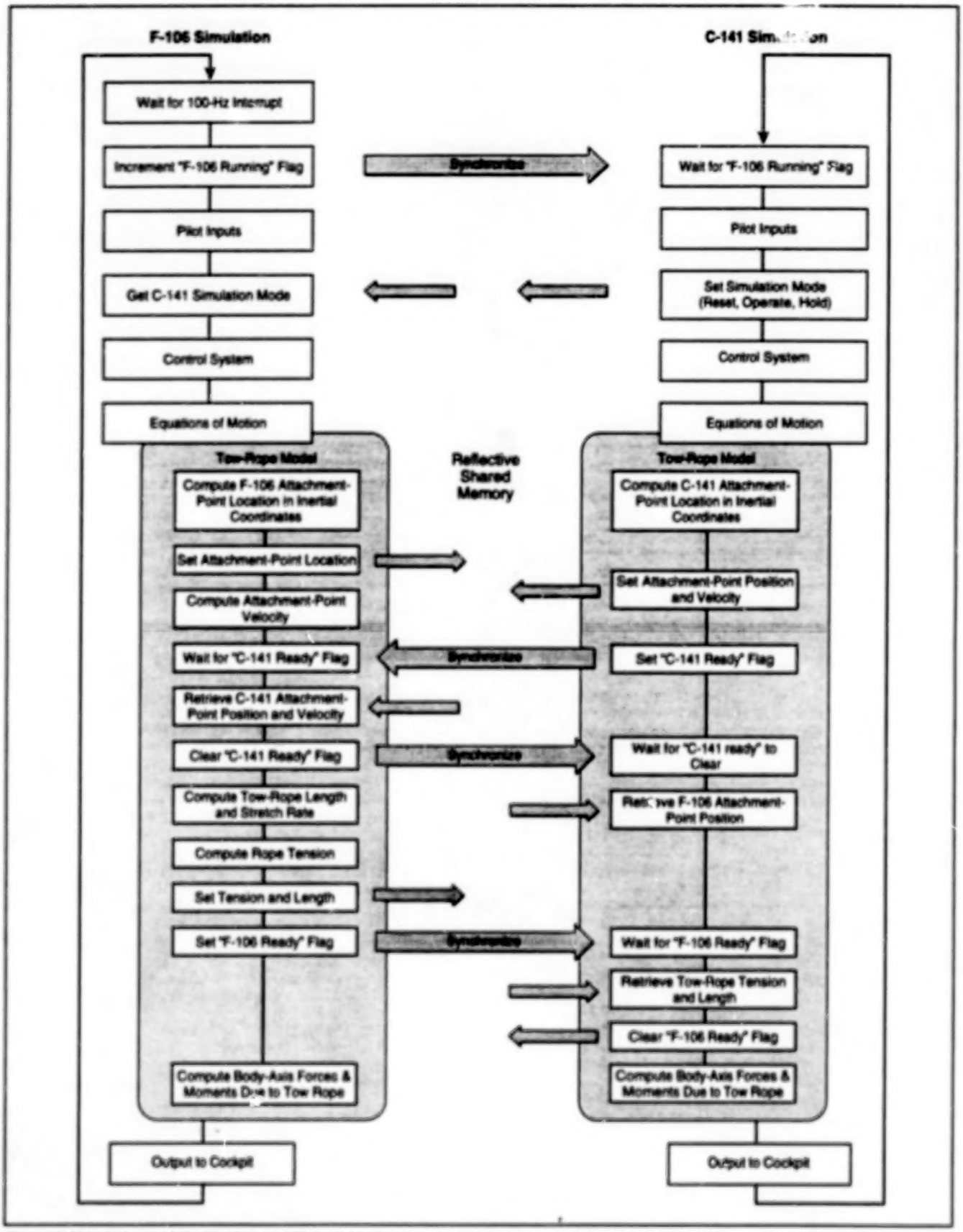

Figure 2. Simulations of the Towing and Towed Airplanes were synchronized to obtain consistent results.

firmed the results of the F-106 simulation. The assumption that the C-141 airplane could be treated as a point mass turned out to be a good one. The C-141 pilot could not feel the effects of the F-106 doing normal small-amplitude maneuvers on tow.

The availability of two independent simulations also afforded a capability to achieve quicker, more productive, simulation sessions. Instead of generating a C-141 trajectory and then preparing and

transferring the resulting data for playback in the F-106 simulation, the C-141 pilot could simply hit a "simulation reset" button and immediately try a different takeoff profile. This enabled the F-106 test pilot to quickly get the feel of the towed operation, and soon this pilot's task became easy. This setup also proved valuable for evaluating various failure scenarios during full mission simulation with the control room being fed by a stream of data generated by the simulator and transmitted by pulse-code modulation.

Six towed flights were performed in a demonstration program that was completed on February 6, 1998. Extensive instrumentation was used so that flight results could be compared with simulation results. It turns out that the simulation tow model was good at predicting rope tension, but a little conservative in predicting stability. The F-106 pilot was able to fly to more extreme tow angles before encountering the divergent oscillations. Part of this difference between the simulation and the flight tests may be due to the assumption of a straight tow rope in the simulation. During the flight tests, the tow rope would "sail" and develop significant curvature. In later flights, the tow rope was marked at regular intervals and video images were recorded so that this phenomenon could be studied in more detail. With the flight-instrumentation data and video images, it should be possible to develop a more realistic tow-rope model that can be incorporated into the simulation.

This work was done by Ken Norlin and Jim Murray of **Dryden Flight Research Center** *and Joe Gera of Analytical Services and Materials, Inc. Further information is contained in a TSP [see page 1].*
DRC-98-33

Lightweight "Beach-Ball" Robotic Vehicles

These rovers could be driven by wind and/or internal electric power.

NASA's Jet Propulsion Laboratory, Pasadena, California

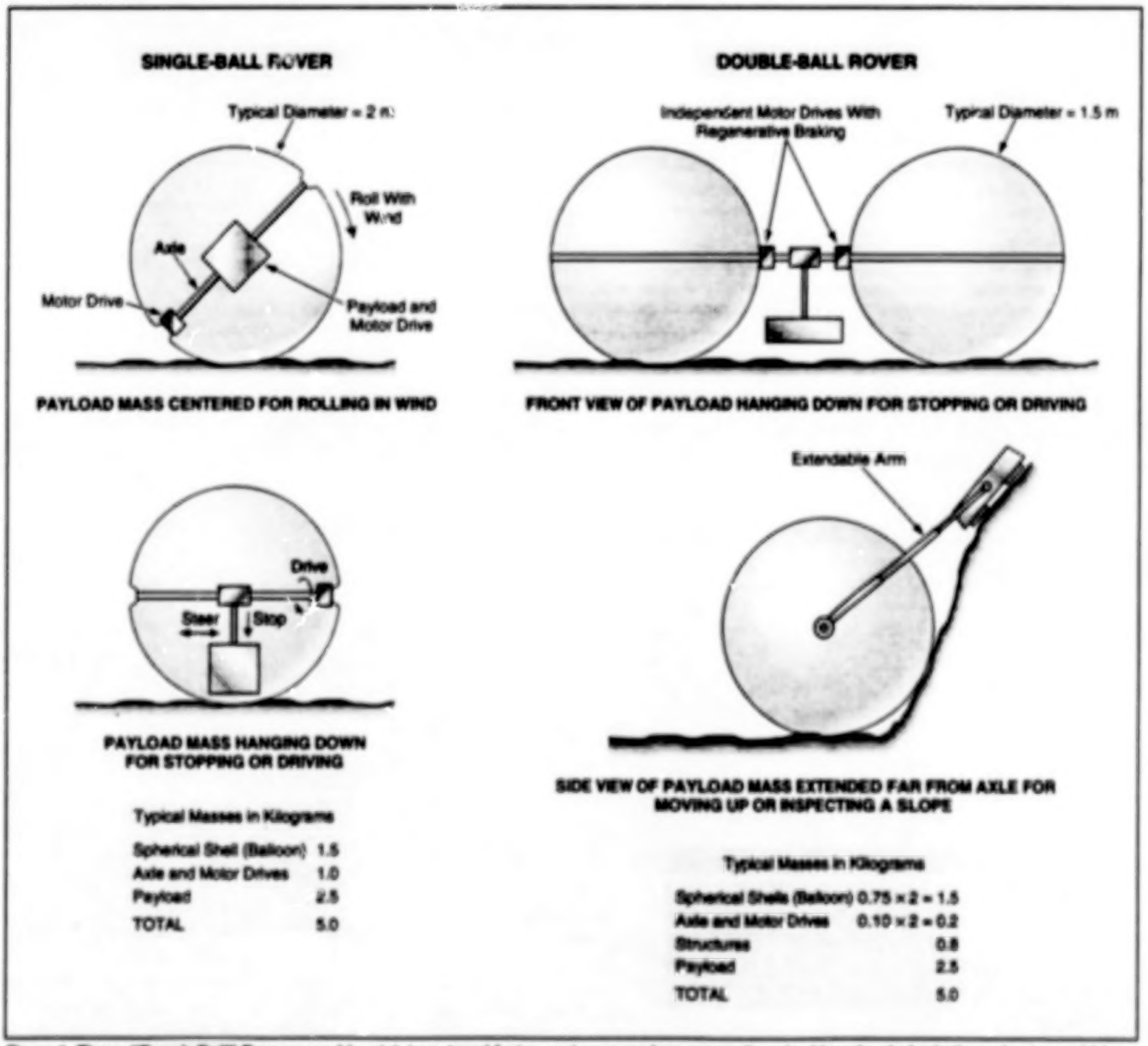

Figure 1. These "Beach-Ball" Rovers would weigh less, travel faster, and consume less power than do older wheeled robotic exploratory vehicles.

Figure 2. A Working Three-Wheeled Inflatable Rover with an upper simulated photovoltaics sphere has been enlarged fourfold to show anticipated size for a lightweight Mars rover.

Lightweight, inflatable robotic vehicles (rovers) that superficially resemble beach balls and that could be driven by wind and/or electric power are undergoing development. These rovers were conceived for carrying scientific instruments across rocky terrain on Mars, and are intended to move faster, weigh less, and consume less power than do the wheeled robotic vehicles that have been used in planetary exploration until now. Given their resemblance to beach balls in both appearance and function, these rovers have obvious potential for adaptation to terrestrial use, especially as toys.

One previous "beach-ball" rover concept was that of an uncontrolled rover little different from an ordinary beach ball. Another previous concept was that of a spherical balloonlike shell, within which motor-driven weights would be moved along internal diametral tethers to shift the center of gravity to make the shell roll [this concept was described in "'Beach-Ball' Robotic Rovers" (NPO-19272), *NASA Tech Briefs*, Vol. 19, No. 11, (November 1995), page 83.]

The present concept differs from both previous concepts, though it incorporates some elements of both. The present concept encompasses both single- and double-ball rovers (see Figure 1). A single-ball rover would contain a diametral rod that would serve as an axle. A payload-and-motor-drive assembly could move itself along or across the axle. To enable the ball to roll freely in the wind, the payload mass would be centered in the ball. To stop or prevent rolling, the payload mass would be shifted away from the center, either along or across the axle. With the payload mass hanging down from the axle, another motor drive at one end of the axle could exert torque on the ball to make the ball roll in the absence of wind. Steering could be effected by moving the payload left or right along the axle during rolling or driving.

In a double-ball rover, the balls would be connected by an external axle collinear with their internal axles. The payload-and-motor-drive assembly would be mounted on the external axle. Both balls would be equipped with independent end-of-axle motor drives similar to those of a single-ball rover, for driving or steering. The double-ball rover could roll with the wind or move under its own power, similarly to a single-ball rover. In addition, the external payload mass could be extended far from the external axle to obtain additional torque to climb a rock or a steep slope. A variation of this design has been fabricated and tested with the extendable arm connected to a "slave" wheel that is pulled behind the two drive wheels (see Figure 2).

This work was done by Jack Jones and Andre Yavrouian of Caltech for **NASA's Jet Propulsion Laboratory**. *Further information is contained in a TSP [see page 1].*
NPO-20283

Laser Anemometer Measures Flow in a Centrifugal Compressor

High-resolution data are representative of flows in practical centrifugal compressors.

Lewis Research Center, Cleveland, Ohio

Detailed measurements of complex flow fields within the NASA Low Speed Centrifugal Compressor (LSCC) have been acquired. The measurement data provide insight into the fundamental physics of flow in centrifugal compressors, and can be used to assess computational fluid dynamics codes and to develop flow-physics models. The resultant benefit is better predictive computational tools and shorter design cycle times.

Centrifugal compressors are widely used in auxiliary power-unit turbochargers, small gas turbine engines, gas-processing plants, and other applications. However, in comparison with their axial-flow counterparts, centrifugal compressors have generally been investigated in less detail.

The LSCC was designed to be representative of conventional high-speed subsonic compressors typically employed in small gas turbine engines. However, the measurements were acquired in the LSCC at low subsonic speeds, where the flowing air behaves as though it were essentially incompressible. As such, the measurements are reasonably representative of what would be found in many centrifugal pumps. The measurement data can therefore be used to validate any aerodynamical computer code that is applicable to centrifugal pumps.

The large size and low speed of the LSCC enable the detailed measurement, by use of a laser anemometer, of all three components of velocity within passages between rotor blades, with a spatial resolution unparalleled in investigations of high-speed compressors. For example, three-dimensional viscous flows that occur very near the surfaces of blades were measured in detail. Complementary measurements of static pressures on blade and shroud surfaces, pressure measurements by pneumatic probes at various positions across inlet and exit surfaces were acquired, and flow-visualization tracings were also acquired. Collectively, the results of the experiments in the LSCC constitute a benchmark set of high-quality data for assessing the predictive capabilities of state-of-the-art three-dimensional viscous-flow computer codes.

Figure 1 illustrates the LSCC impeller and the locations of laser-anemometer measurements. The upper part of Figure 2 shows results of velocity measurements taken at the 64-percent meridional chord position, indicating the extent of the through-flow-velocity deficit characteristic of centrifugal-compressor flow fields. The lower part of Figure 2 illustrates the nature of secondary flow mea-

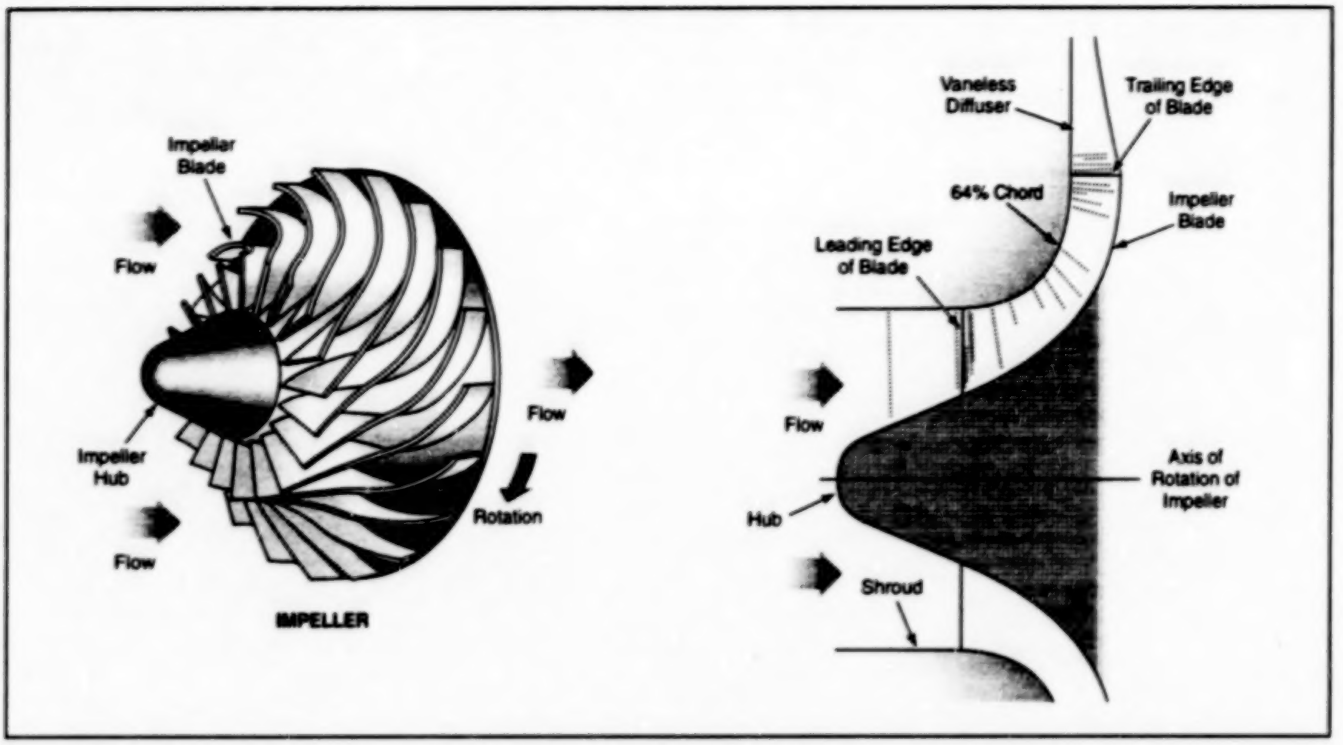

Figure 1. The **Dots Indicate Locations**, most within the passages between rotor blades, where flow velocities were measured by a laser anemometer.

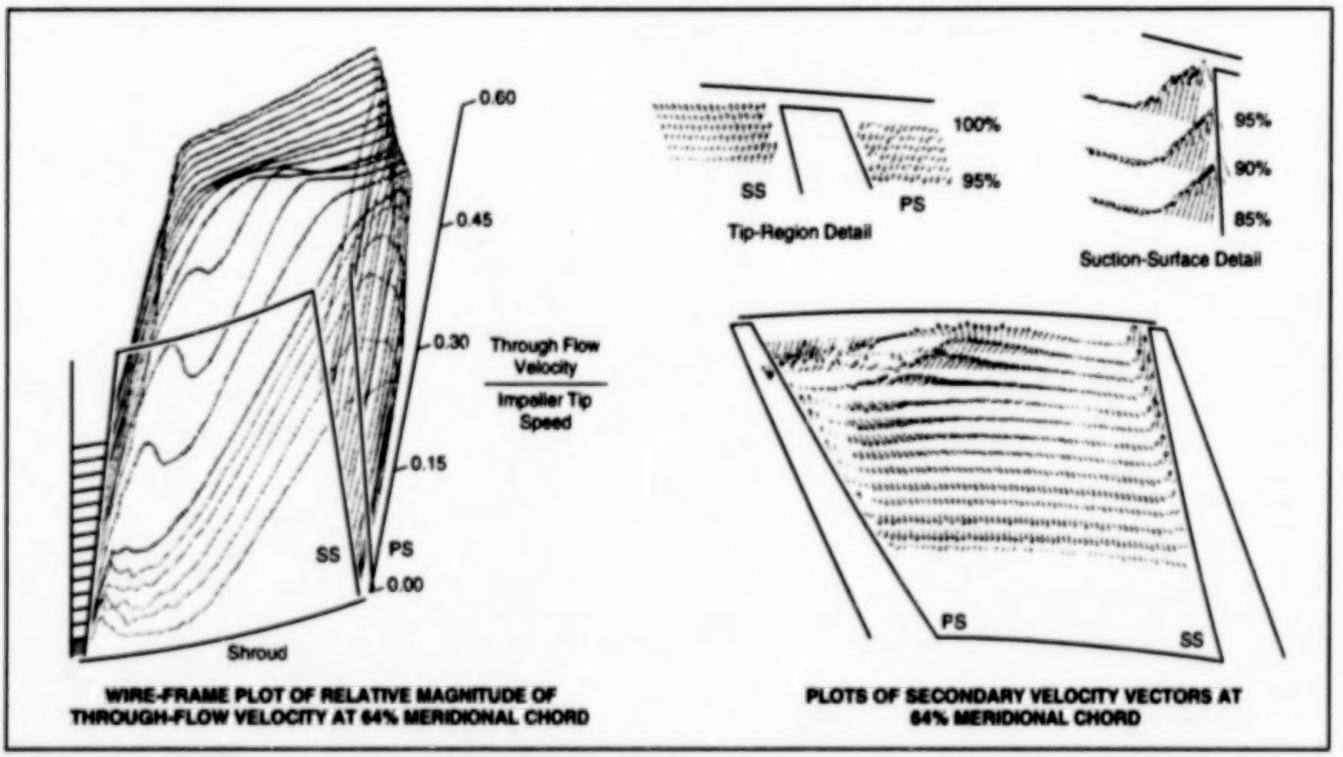

Figure 2. **Selected Results of Velocity Measurements** illustrate the general nature of the data acquired. "PS" and "SS" denote the pressure and suction surface, respectively, of a rotor blade. For clarity, different vector scales are used in the main and detail plots of velocity vectors, and the pitchwise spatial resolution of the main plot is 1/3 that of the detail plots.

surements at the same location, along with some details that demonstrate the resolution of measurements acquired in viscous-flow regions near blade surfaces.

This work was done by Randall M. Chriss, Anthony J. Strazisar, and Jerry R. Wood of **Lewis Research Center** *and Michael D. Hathaway of the U. S. Army Research Laboratory. Further information is contained in a TSP [see page 1].*

Inquiries concerning rights for the commercial use of this invention should be addressed to NASA Lewis Research Center, Commercial Technology Office, Attn: Tech Brief Patent Status, Mail Stop 7–3, 21000 Brookpark Road, Cleveland, Ohio 44135. Refer to LEW-16417.

Microscopic Heat Exchangers, Valves, Pumps, and Flowmeters

Forced-flow heat-transfer systems would be made by micromachining.

NASA's Jet Propulsion Laboratory, Pasadena, California

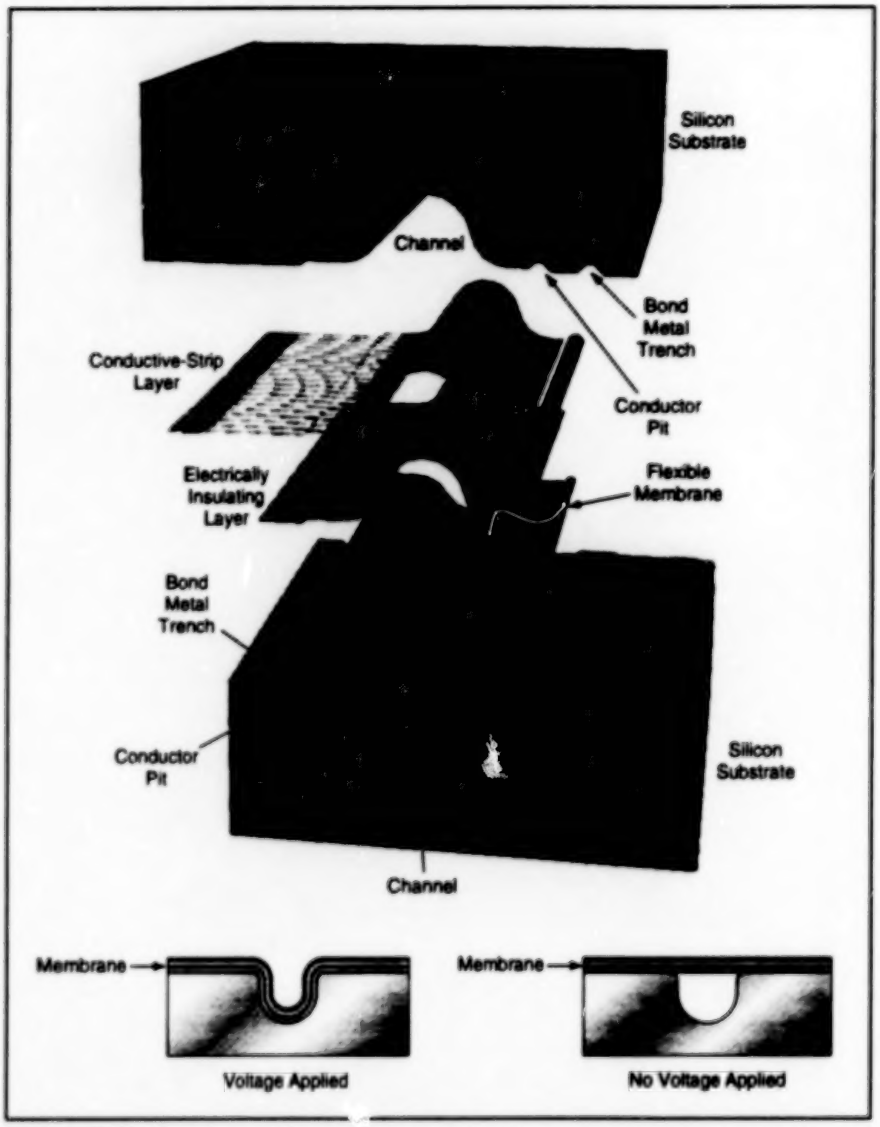

Electrostatic Attraction would be used to pull the flexible membrane into, across, and along the channels: this would generate peristaltic waves in the membrane to pump a fluid along the channel.

Microscopic forced-flow heat-transfer systems containing heat exchangers, flow channels, electrostatically driven peristaltic pumps, and related components have been proposed. These systems would be made largely of silicon, by use of micromachining processes similar or identical to those used to make integrated circuits. These microscopic heat-transfer systems could thus be made as integral parts of integrated circuits: For example, charge-coupled-device (CCD) imaging circuits in infrared cameras could be cooled very effectively by incorporating such systems to circulate cryogenic fluids within the CCD substrates.

The figure illustrates a dual-cavity push-pull embodiment of an electrostatically driven peristaltic pump. The pump channels would be etched into silicon substrates, which are bonded together with an electrically conductive flexible membrane sandwiched between them. The channels would be lined with electrically conductive strips covered with electrically insulating material and separated from each other by electrically insulating barriers. By applying a suitable voltage between the membrane and the conductive strips of each channel in succession, one would cause the membrane to be electrostatically pulled into the channel at successive positions along the channel. Dual interlaced and interlocked shift registers enable alternate inversions of bit-stream sequences and multiple membrane "bubbles" that move down the channel, pushing entrapped fluid in front of each membrane "wall" and pulling the fluid behind each membrane "wall." This pump architecture represents a true two-dimensional analog of a peristaltic mechanism that is valveless, impervious to gas-bubble entrapment, does not require priming, and is self purging. The device is a digital pump that may be single-stepped to function as a valve or, by counting the number of clocked bits, is a precision flowmeter.

A heat exchanger consisting of micromachined channels in a thermally conductive material would be designed to maximize heat-transfer surface area and to provide effective convective coupling of heat between the pumped fluid and the channel surfaces at the expected flow speeds. The use of microscopic channels would make it possible to achieve low conduction and convection losses, with consequent high thermal coupling and short characteristic times for decay of thermal transients.

This work was done by Frank T. Hartley of Caltech for ***NASA's Jet Propulsion Laboratory.*** *Further information is contained in a TSP [see page 1].*

This is the invention of a Caltech/JPL employee, and a patent application has been filed. Inquiries concerning license for its commercial development may be addressed to the inventor:

Frank Hartley
JPL
MS 125-177
4800 Oak Grove Drive
Pasadena, CA 91109
(818) 354-3139

Refer to NPO-19093, volume and number of this NASA Tech Briefs *issue, and the page number.*

Procedure for Designing Safe Robots

Engineering compromises between performance and safety can be made systematically.

John F. Kennedy Space Center, Florida

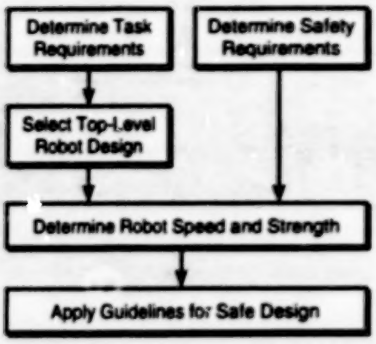

Figure 1. This Five-Step Procedure implements the methodology for designing safe robots.

A methodology for designing robots provides for satisfying both safety and performance requirements. Heretofore, most robot-design efforts have been focussed on maximizing performance, with only incidental regard for safety, under the assumption that humans and delicate equipment would be excluded from robot workspaces during robotic operations. The present methodology was developed out of recognition of the need to ensure safety for humans while realizing the potential ability of robots and humans working together to perform a broader spectrum of tasks than either can perform alone.

The methodology is implemented by a formal design procedure in which quantitative evaluations are performed to effect compromises between the inevitably competing demands of performance and safety. The procedure comprises five main steps and a number of sub-steps (see Figure 1).

The first two steps, which can be simultaneous, are the determination of task requirements and the determination of safety requirements. "Task requirements" as used here denotes such quantitative performance specifications as robot-tip velocities, robot payloads, robot position and force accuracies, and measures of robot dexterity. For a given application and task, minimum acceptable values can be assigned to these specifications to quantify minimum acceptable performance.

"Safety requirements" as used here denotes the set of all robot-performance measures that are related to safety in that they indicate degrees to which robots can harm humans. Such measures include robot static and impact contact force, robot static and impact

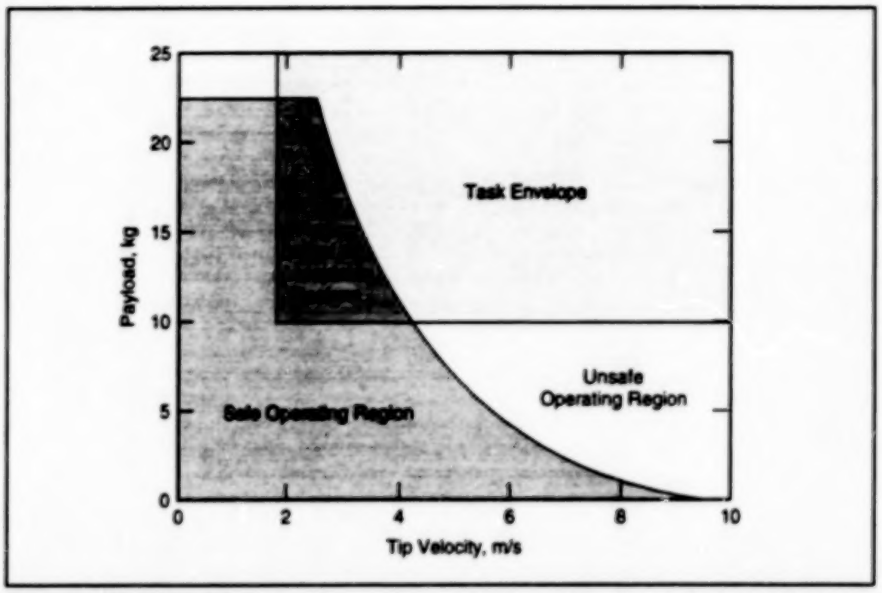

Figure 2. This Safety Diagram with superimposed task envelope for a typical robot illustrates the margin available for designing to satisfy both safety and performance requirements. The intersection of the design and safety envelopes represents the ranges of tip-velocity and payload values of acceptable designs.

vise or pinch forces, robot static and impact contact forces, and crushing forces from robot weights. For a given application and task, maximum allowable values can be assigned to these measures to specify safety limits.

The next step is the selection of the top-level robot design. More specifically, this means the selection of the kinematics, range of motion, and geometry of a robot to accomplish the task as specified in the first step.

In the following step, one determines measures of the speed and strength of the robot on the basis of the top-level robot design and the safety requirements. This step is divided into the following four substeps:

1. Develop mathematical models of robot forces, velocities, and energies to relate design parameters to safety and performance variables.
2. Using the models developed in substep 1, make a safety diagram, which is a plot showing the boundary (denoted the "safety envelope") between safe and unsafe values of two or more safety-related performance measures. Also plot the boundary (denoted the "task envelope") of the task requirements for these performance measures on the safety diagram (see Figure 2).
3. Select target performance specifications (e.g., a value of tip velocity and a value of payload weight) that lie within the intersection of the safety and task envelopes.
4. Select the joint torques and velocities needed to achieve the target performance specifications and design the robot joints and actuators accordingly.

The last step is the application of guidelines for safe design. Six guidelines have been formulated through analysis of those safety and task specifications that are mutually independent (or at least nearly so). Each guideline represents a strategy for independently optimizing some aspect of either safety or performance.

The guidelines are the following:

1. Maximize robot accuracy,
2. Maximize robot dexterity.
3. Minimize robot weight.
4. Eliminate pinch points and maximize potential vise radii.
5. Maximize robot contact area.
6. Maximize robot padding thickness.

These guidelines, if followed during the design process, can help ensure a high-performance, safe robot design.

This work was done by Karl T. Ulrich, Timothy D. Tuttle, Joseph P. Donoghue, and William T. Townsend of Barrett Technology, Inc., for **Kennedy Space Center.** *Further information is contained in a TSP [see page 1].*

In accordance with Public Law 96-517, the contractor has elected to retain title to this invention. Inquiries concern-

ing rights for its commercial use should be addressed to
William T. Townsend
Barrett Technology, Inc.
139 Main Street
Kendall Square
Cambridge, MA 02142
(617) 252-9000

Refer to KSC-11849, volume and number of this NASA Tech Briefs *issue, and the page number.*

Miniature Side-Bore Sample-Acquisition Mechanism

This mechanism could withstand large deceleration and would function in extreme cold.

NASA's Jet Propulsion Laboratory, Pasadena, California

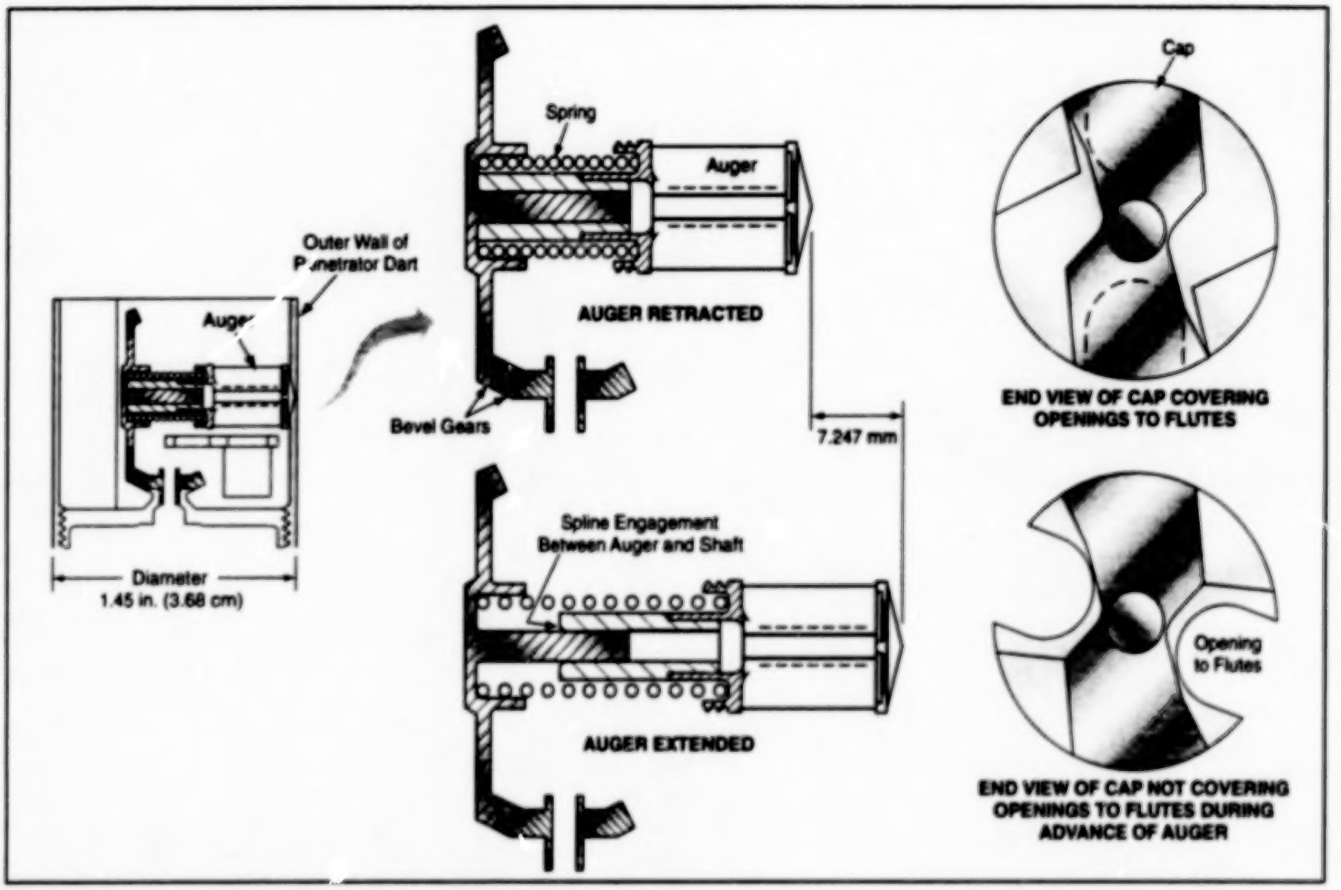

The Entire Mechanism Would Fit within the penetrator dart.

The figure illustrates various aspects of a proposed mechanism that would be mounted in an instrumented penetrator dart for use in acquiring a sample of soil. In operation, the dart would be dropped from a height to make it penetrate the ground to a suitable depth, then the mechanism would be activated to acquire the sample of soil through the side of the dart. The mechanism and dart would be built to withstand a ground-impact deceleration of as much as 30,000 times the acceleration of normal Earth gravity. The mechanism would be able to take a sample of relatively hard, frozen soil at a temperature as low as –80 °C. Originally designed for use in remotely controlled exploration of Mars, the penetrator and mechanism might be adaptable to sampling soil in remote, cold, or otherwise hostile or inaccessible environments on Earth.

The mechanism would include an auger with its axis perpendicular to that of the dart. During transport and impact, the auger would remain stowed within the dart. During the sample-acquisition process, the auger would be pushed out from the dart and turned, thereby boring a side hole and drawing soil into the dart for sampling.

A brushless dc motor would be coupled through a right-angle bevel-gear drive to a shaft for turning the auger. The auger would be free to slide axially along the shaft, but a square spline would constrain the auger to rotate with the shaft. The auger would be spring-loaded toward extension, but prior to use, it would be restrained against extension by engagement between mating threads on the auger and an interior structural component of the dart.

To prevent the flutes of the auger from ingesting soil before reaching the desired depth, the openings to the flutes would be covered by a drill cap during transport and impact. During the first 70° of rotation of the auger, the drill cap would not rotate; thus, the auger would rotate relative to the cap, bringing the openings to the flutes out from under the cap. Upon reaching 70°, the auger would engage the cap; thereafter the auger and cap would rotate together, so that the openings to the flutes would remain exposed.

This work was done by Tommaso P. Rivellini and Christopher J. Voorhees of Caltech for **NASA's Jet Propulsion Laboratory**. *Further information is contained in a TSP [see page 1].*
NPO-20163

National Aeronautics and
Space Administration

END

09/09/98